Development and Characterization of Solid-Contact Paper-Based and Micro Ion-Selective Electrodes for Environmental Analysis

2018

Stephanie Armas
University of Central Florida

DEVELOPMENT AND CHARACTERIZATION OF SOLID-CONTACT PAPER-BASED AND MICRO ION-SELECTIVE ELECTRODES FOR ENVIRONMENTAL ANALYSIS

by

STEPHANIE MICHELLE ARMAS
B.S. University of Central Florida, 2016
B.S. University of Central Florida, 2016

A thesis submitted in partial fulfillment of the requirements
for the degree of Master of Science
in the Department of Chemistry
in the College of Sciences
at the University of Central Florida
Orlando, Florida

Summer Term
2018

Major Professor: Karin Y. Chumbimuni-Torres

ABSTRACT

Ion-selective electrodes (ISEs) have extensively been used for food analysis, as medical diagnostic tools, and for some environmental applications. However, ISEs are hindered by the need of a bulky reference electrode and the pre-conditioning step of the sensor, which can often be lengthy. This work will discuss how the direct addition of target analyte into the cocktail sensing membrane can circumvent the pre-conditioning step. Furthermore, the work is presented in an optimized ready-to-use single strip design, where the bulky glass reference electrode (RE) is no longer needed. The bulky RE was replaced by drop casting a simple two-component mixture consisting of the co-polymer methyl methacrylate-co-decyl methacrylate and the ionic liquid 1-Ethyl-3-methylimidazolium bis (trifluoromethane sulfonyl) amide. Furthermore, this work will also highlight the benefits of solid-contact ISEs, specifically focusing on two solid-contact platforms: 1) paper-based and 2) a micro-electrode platform. Paper-based based sensors were designed to be used as a possible diagnostic tool to be implemented in undeveloped countries to monitor low levels of potassium and iodide, as model ions. The micro(μ) ISEs were applied for the *in-situ* analysis of zinc in citrus plants as a mean to monitor and assess disease progression or therapy.

“Basically, I have been compelled by curiosity.”

-Mary Leakey

To my mother for all her love, guidance and support throughout this journey.

ACKNOWLEDGMENTS

This work was supported by the Office of Undergraduate Research at the University of Central Florida as well as by Citrus Disease Research and Extension (CDRE) (grant no. 2016-70016-24828/project accusation no. 1008984) from the USDA National Institute of Food and Agriculture. Any opinions, findings, conclusions, or recommendations expressed in this publication are those of the author(s) and do not necessarily reflect the view of the U.S. Department of Agriculture. My sincerest gratitude to the McNair program for the financial and personal support throughout my graduate education. A special thanks to Michael Aldarondo-Jeffries, Natalia Toro, Arlene Ollivierre and Katherine Thompson for all their help, advising and support!

I would like to extend my gratitude to my mentor Dr. Karin Chumbimuni-Torres who gave me the opportunity to join the Nanobioelectrochemistry (NBEL) lab, a woman who has taught me so much, entrusted me with a high degree of responsibility and has helped me achieve unimaginable goals. A special thank you to Dr. Santra for his support and advice during this project, providing great insight to tackle the zinc problem, and for sharing his knowledge about citrus greening disease to me and our laboratory. Similarly, many thanks to Dr. Woo Hyoung Lee for a great collaboration and extensive share of knowledge from an engineering perspective. Sincerest thanks Dr. Beazley for her support throughout my graduate studies and for taking the time to serve as a committee member. Thank you for all the support and training given by Dr. Percy Calvo-Marzal. Lastly, my sincerest gratitude to all members of the NBEL who made my time in lab enjoyable and fun. A special thank you to Andrew Manhan, Olivia Younce, Cody Autrey,

Enrique Blanco, Andrea Bances-Monard for all you hard work and support. Additionally, Dawn Mills and Parth Patel for the great research collaboration, support, and great friendship! I express the greatest gratitude to my biggest support, my best friend, and my motivation, my mother. She has put up with my anxiety, late nights and mood swings from this journey. I love you very much! Finally, thank you to all my family and friends who have guided me and supported me to prevail in my degree.

TABLE OF CONTENTS

LIST OF FIGURES

LIST OF TABLES

LIST OF ACRONYMS/ ABBREVIATIONS

$(CH_3)_2CO$	Acetone
$[C_2mim]^+$	1-ethyl-3-methylimidazolium
$[NTF_2]^-$	Bis (trifluoromethane sulfonyl) amide
µ	Micro
AAS	Atomic Absorption Spectroscopy
AIBN	2,2’ azobis(isobutyronitrile)
aq	Aqueous
C_1	Concentration of Target Analyte at X_1
C_2	Concentration of Target Analyte at X_2
Ca. L. Laf	Candidatus Liberibacter Africanus
Ca. L. Lam	Candidatus Liberibacter Americanus
Ca. L. Las	Candidatus Liberibacter Asiaticus
$CaCl_2•2H_2O$	Calcium chloride dihydrate
CGD	Citrus greening disease
$CHCl_3$	Chloroform
Cu	Copper
D	Diffusion Constant
DBL	Diffusion Boundary Layer
DCM	Methylene Chloride
DOS	Bis(2-ethylhexyl) sebacate

E°	Standard Potential
EMF	Electromotive Force
E_{PB}	Phase Boundary Potential
F	Faraday's Constant
H_2SO_4	Sulfuric Acid
HCl	Hydrochloric Acid
HLB	Huanglongbing
HNO_3	Nitric Acid
I	Primary ion
ICP-AES	Inductive Coupled Plasma - Atomic Emission Spectroscopy
IL	Ionic Liquids
ISE(s)	Ion-Selective Electrode(s)
J	Net Flux
KCl	Potassium Chloride
KI	Potassium Iodide
KTFPB	Potassium [3,5-bis(trifluoromethyl)phenyl] borate
L	Ionophore/ligand
LC	Liquid-Contact
LiCl	Lithium Chloride
LOD	Limit of Detection
Log $K_{I,J}^{pot}$	Selectivity Coefficient of Primary Ion I, Against Interfering Ion J
M	Molarity

M^+	Lipophilic Cation
MC3	[9]-Mercuracarborand-3
MIFE	Microelectrode Ion Flux Estimation
MMA-DMA	Methyl Methacrylate co-Decyl Methacrylate
mV	Millivolts
n	Stoichiometric number
$Na(NO_3)_2$	Sodium Nitrate
NaCl	Sodium Chloride
NaI	Sodium Iodide
NaIX	4-tertbutylcalix [4]arene-tetracetic acid tetraethyl ester
NaOH	Sodium Hydroxide
NaTFPB	Sodium [3,5-bis(trifluoromethyl)phenyl] borate•
o-NPOE	*Ortho*-nitrophenyl octyl ether
org	Organic
PBSC	Paper-Based Solid Contact
POC	Point of Care
POT	Poly(3-octylthiophene-2,5-diyl)
PVC	Polyvinyl Chloride
R^-	Lipophilic Anion
R	Universal Gas Constant
RE	Reference Electrode
SC	Solid-Contact

SWCNTs	Single Walled Carbon Nanotubes
T	Temperature
$TDMANO_3$	Tridodecylmethylammonium nitrate
THF	Tetrahydrofuran
TMSDMA	N-N dimethyltrimethyl-silyamine
X	Distance from Surface of Plant Tissue
z	Charge
Zn	Zinc
$Zn(NO_3)$	Zinc Nitrate
ZnI	Zinc Ionophore I / Tetrabutylthiuram Disulfide
ZnO	Zinc Oxide

CHAPTER ONE: INTRODUCTION AND LITERATURE REVIEW

1.1 Motivation

The development and distribution of inexpensive, low energy, flexible and portable devices for in-field and point-of care (POC) testing, are now a necessity for marginal areas and underdeveloped countries, where institutions are often swamped with patients and needed exams cannot be done in time. Similarly, due to low economical resources and lack of water control, high levels of toxic metals can be found in drinking water and soil. Ion-selective electrodes (ISEs) are considered to be promising field deployable tools that possess the necessary qualities for performing analysis in drinking water and other matrices. ISEs possess a high degree of versatility, selectivity and availability to perform trace level analysis similar to well established methods [1,2]. They are a class of potentiometric sensors, which operate at zero current conditions and have been around since 1906, were the popularly known pH glass electrode was discovered by Max Cremer [3]. Other types of ISEs, like crystalline and polymer- based ISEs soon followed in the early and mid-1960s. Here, focus will be made on polymer-based ISEs, due to their ability to detect a wide range of ions in comparison to the former discussed ISEs. Although much research has been done to optimize polymer-based ISEs, [4-6] understanding the transduction mechanism of new solid-contact platforms (discussed in item 1.3), development of robust calibration free electrodes and preparing all-solid-state calibration free ISEs still remains a challenge for commercialization purposes. Thus, optimization of phase boundary potential via development of new transduction materials still leaves ample room for research prior to commercialization. This thesis will discuss the optimization of ISE conditioning protocol

adapted to a solid-contact (SC) platform, as well as the incorporation of a simple, paper-based, flexible platform for in-field analysis discussed in chapter two. The application of ISEs was further extended to monitor zinc uptake in citrus plants, inspired by the widespread of citrus greening disease, affecting crops across the country and worldwide, leading to millions in revenue loss [7,8]. The characterization, optimization and application of the micro-electrode platform will be discussed in chapter three. Consequently, this section will cover the response mechanism and theory behind ISEs and reference electrodes, as well as the main two platforms of polymer-based ISEs, solid-contact and liquid-contact.

1.2 ISE Response Mechanism and Theory

Broadly, ISEs are tools which measure the activity of ions quantitatively following the Nernst equation. To broaden the versatility and selectivity of these tools, polymer-based ISEs came about in the mid-1960s[3]. As the name describes, they are composed of a polymer matrix, which provides the support and mechanical stability needed to function. The polymeric membrane is composed of a lipophilic ion-exchanger ($M^+ R^-$) that ensures electro neutrality and provides perm selectivity, allowing ions to be exchanged with the aqueous solution and avoiding the extraction of counter anions into the membrane, respectively[9]. Employing solely an ion-exchanger and plasticized polymer can lead to a Nernstian response, contingent upon that the solution to measure contains only the primary ion. A sub-Nernstian response (mixed ion response) will be obtained if there are interfering ions present in the measuring solution because the activity of the primary ion in the organic phase will be decreased. To improve the poor selectivity, a neutral carrier, or ionophore (L) is added to the membrane. The ionophore would selectively bind to the target ion, highly

improving the selectivity of the system. The earliest work was pioneered by Moore and Pressman with the antibiotic and ionophore known as valinomycin, which exhibits high selectivity for potassium ions [3,9]. Several ionophores were then developed to expand detection to a variety of ions, including heavy metals [3,9].

To exhibit the desired potential response, also known as the electromotive force (EMF), there are two main conditions that must be met. First, ensure that the activity of the primary ion in the organic membrane is kept constant and is independent of sample composition. Second, ensure that all contributions to the EMF response are sample independent, with the exception of the phase boundary potential. The phase boundary potential, $E_{PB,}$ is achieved at the interface between the organic and aqueous phase, yielding a separation of charges as seen in Figure 1. The resulting EMF is the sum of all phase boundary potentials and can be simply expressed as the well-known Nernst equation, eq.:

$$EMF = E^0 + \frac{RT}{z_i F} lna_i = E^0 + \frac{2.303RT}{z_i F} loga_{i,\mathrm{aq}} \quad (1)$$

Where, E^0 is the standard potential, z and a are the charge and activity of primary ion, i, respectively. R is the universal gas constant, T is the absolute temperature and F is Faraday's constant.

To satisfy the first condition, the ratio of ionophore to ion-exchanger must be optimized to leave a substantial concentration of free ionophore. The stoichiometric binding of ionophore to target analyte dictates the optimization of ionophore to ion-exchanger concentration added to the membrane. For instance, valinomycin, exhibits a 1:1 binding ratio; thus, a 2:1 ionophore to ion-exchanger ratio is required to satisfy the first condition. Essentially, by having half of the ionophore unchelated, the activity of the primary ion in the organic phase becomes impervious to

the sample analyte, and a buffer system is created between the organic and aqueous phase, satisfying the second condition [3,9]. To chelate the ionophore with the ion of interest, the membrane is exposed to the primary ion solution for a period of ~12-72 hours depending on the analyte [7]. This is known as the conditioning protocol, wherein the cation from the ion-exchanger in the organic phase (in the case of a cation-exchange membrane) exchanges with the cation in the bulk solution containing the primary ion, until equilibrium is reached. Although efforts have been done to minimize such time [11], this thesis, will farther discuss a medium by which to circumvent this tedious process in chapter two.

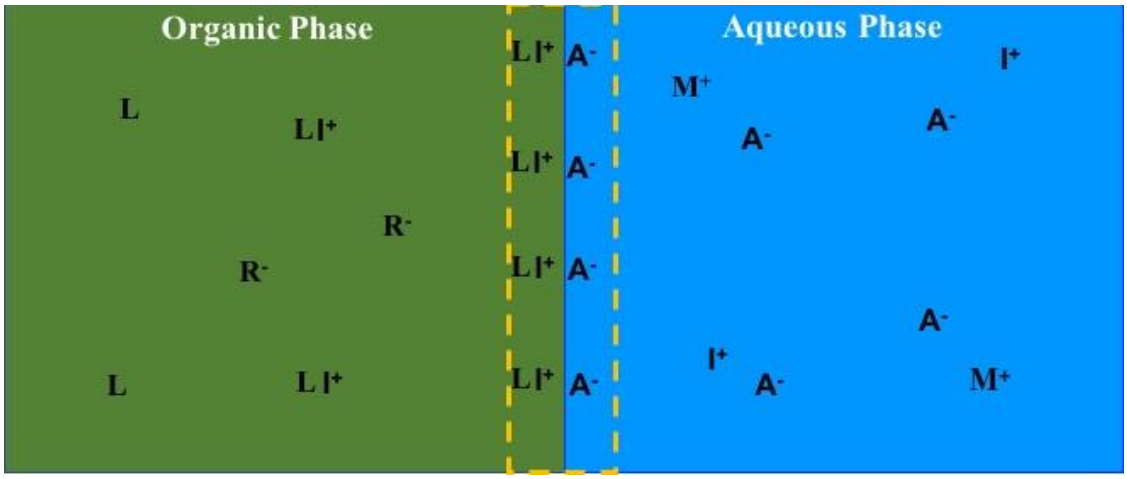

Figure 1. Equilibrium distribution of doped-ionophore based polymeric membrane with aqueous bulk

Another important component in an ISE measurement is the reference electrode (RE). The RE is responsible for maintaining a stable and well-known potential in an electrochemical cell. A traditional potentiometric measurement set-up can be seen in Figure 2, where the ISE is coupled with a RE to retrieve an EMF response, that is derived from the potential difference between the connection of the ISE and the RE [3].

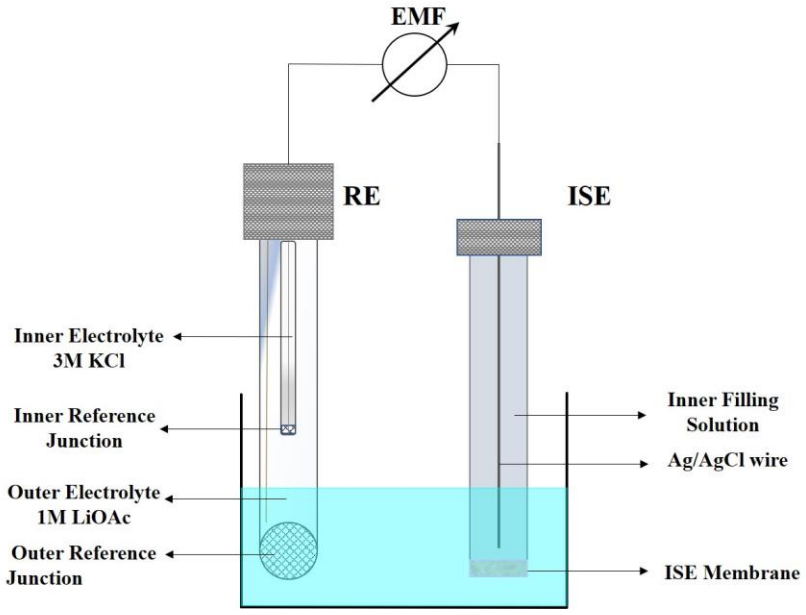

Figure 2. Traditional ISE measurement set-up

1.3 Polymer-Based ISE Platforms: Liquid-Contact vs Solid-Contact ISEs

The type of ISE shown in Figure 2 displays a liquid-contact ion selective electrode, indicating that a solution containing the primary ion (target ion) is in direct contact with the ion-selective membrane, and a Ag/AgCl wire is in contact with a chloride solution to allow for the transduction of the ionic to electronic (potential) signal to take place. Unfortunately, this system comes with some disadvantages, especially for environmental applications, where the electrode cannot withstand deep ocean measurements, due to high pressure, and miniaturized electrodes suffer from evaporation of inner filling solution and osmotic pressure development across the ion-selective membrane, which would have a negative impact on the response of the ISE [3]. For this reason, solid-contact ion selective electrodes came about in the 1970s to overcome the abovementioned disadvantages of LC-ISEs. Solid-contact ISEs are able to be easily miniaturized, withstand high pressures, can be adapted to various platforms (paper, wire, plastic)

and the elimination of the inner filling solution greatly improved limits of detection [13] Nevertheless, solid-contact ISEs came with their own challenges. The formation of an aqueous layer between the solid substrate and ion-selective membrane led to a poorly defined phase boundary potential and subsequent degradation in sensor response. As a result, a hydrophobic intermediate layer, such as conducting polymers were used to prevent the formation of this electrolyte layer [3,12,13].

In a traditional LC-ISE platform, the transduction mechanism is very well understood and studied. Ionic to electronic transduction is achieved by the reversible redox reaction of $AgCl\ (s) + e^- \rightarrow Ag(s) + Cl^-(aq)$, where the Cl^- concentration is kept constant. This reaction then defines the interfacial potential between Ag/AgCl electrode and inner filling solution, and the charge carrier is the target ion [13]. The transduction mechanism of solid-contact electrodes is not as well understood and has not been studied as much as that of the LC-ISEs. Nevertheless, Bakker [14,15], Bühlmann[13], Michalska [16] , and others[17,18] have begun to shed some light into the transduction mechanism of SC-ISEs. It has been found that SC-ISEs employing a conducting polymer transduce a charge carrier from ions to electrons via the oxidation/reduction of the conducting polymer [13-16], whereas materials such as carbon nanotubes or graphene comes from a double

layer capacitance phenomenon [13,17]. Here, all SC-ISEs will employ poly(3-octylthiophene-2,5-diyl) due to its excellent potential stability and hydrophobic nature, which allows for a more robust platform [15].

1.4 Limits of Detection

For ISEs, the limits of detection as IUPAC states, is calculated by the cross point of two linear regression lines of a calibration curve as seen in Figure 3 [9]. The lower limit of detection arises from two phenomena, 1) perturbation of interfacial sample activity induced by constant diffusion of low ion concentration from the inner filling solution into the sample and 2) interference by competing ions in solution, that is not a "clean" system. To improve lower limits of detection, particularly for LC-ISEs, buffer systems and lower concentrations of inner filling solution were employed, leading to sub micromolar detection limits [9]. Buffer systems work on the principle that a ligand added to the sample will provide a buffering effect by decreasing the concentration of primary ions released from the membrane [9]. Similarly, lower concentrations present in the inner filling solution will also enable lower perturbation of the interfacial sample activity, since there will be less ions available to constantly diffuse through the membrane [9]. SC-ISEs on the other hand, do not suffer from the first phenomena due to the direct contact with conductive substrate. Consequently, nanomolar limits of detection can be achieved [2,4,20-22]. The upper limit of detection for a cation-exchange membrane is derived from a coextraction process that leads to a loss of permselectivity, known as Donnan-failure [9,19]. The upper limit of detection can also be linked to the lipophilic nature of the anion, higher lipophilicity of the anion will lead to a loss of permselectivity sooner. The degree of lipophilicity of cations and anions are illustrated by the Hoffmeister series below, where the top row represents cations degree of lipophilicity decreasing from left to right, whereas it increases from left to right for anions in the bottom row [23.24].

$NH_4^+ > Cs^+ > K^+ > Na^+ > Li^+ > Mg^{2+} > Ca^{2+} > Zn^{2+}$

$SO_4^{2-} > cit^- > OH^- > Cl^- > NO_3^- > ClO_3^- > I^- > ClO_4^- > SCN^- > PF_6^-$

Figure 3. Hoffmeister series

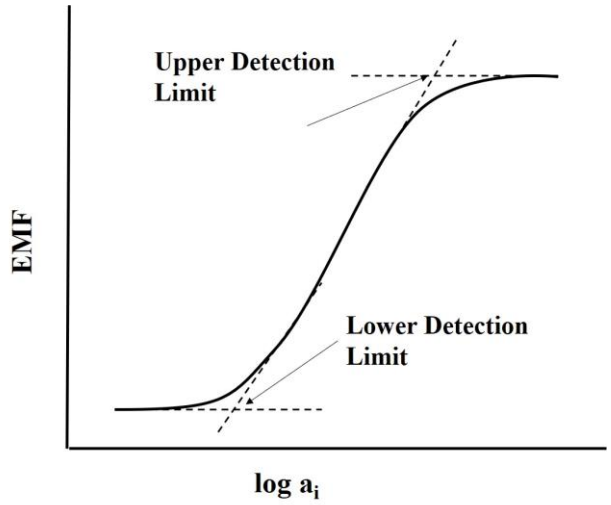

Figure 4. Defining the upper and lower limit of detection of ISEs

1.5 Selectivity Methods

There are two semiempirical selectivity methods recommended by IUPAC, 1) fixed interference method and 2) separate solutions method. Both methods follow the Nicolskii-Eisemann equation, each with its own spin to it [9,25]. A third method, known as the matched potential method does not follow the same equation as above, but was incorporated by Gadzekpo and Christian to provide a more empirical selectivity method, where the selectivity coefficients better reflect real-world sensors [9]. The only catch to this method is that the selectivity coefficients are strictly dependent on experimental conditions and are not constant for a particular electrode. Briefly, the fixed interference method (FIM) is also applicable for real life scenarios, but it does not reflect the "true" selectivity of a ligand to its target ion, as it works under optimal conditions. The separate solution method was employed by comparing two solutions; one solution with only the primary ion and another with only the interfering ion present. When this method first came to be, the electrode was tested under optimal conditions (primary ion in the membrane), wherein a Nernstian response for interfering ions was not observed. This is because it is not

thermodynamically favorable to displace a preferred ion. Furthermore, the Nicolskii-Eisemann formalism requires that each ion under consideration should yield a Nernstian response, which was not the case in the former separate solution method, so the obtained selectivity coefficients were biased. For this reason, a modification to the experimental protocol was brought forth by Bakker [26] which allowed Nernstian responses for interfering ions by exposing the electrode to the least interfering ion first and the primary ion last, eliminating any bias. The Nicolskii-Eisemann equation can be seen below:

$$logK_{IJ}^{POT} = \frac{z_i F(E_j - E_i)}{2.303RT} + \log(\frac{a_i}{a_j^{z_i/z_j}}) \quad (2)$$

Here, z_i and z_j are the charge of the primary ion and interfering ion, respectively. F is faraday's constant, E_j and E_i are the interfering ion and primary ion potential response, a_j and a_i are the corresponding activities. The protocol involves conditioning the developed ISE in a solution of least interfering ion and measure the various ions in order of least interfering to most interfering ion solution (in general, the primary ion is measured at the end). Once the electrode is exposed to the primary ion, it will no longer yield a Nernstian response to the discriminating ion. This method allows true understanding in ligand selectivity behavior and can be readily applied to real-word scenarios [24].

1.6 Microelectrode Flux estimation

Microelectrode flux estimation is a powerful non-invasive technique to perform characterization of ions diffusing through cells membrane, or to study the kinetics of membrane transport processes across cellular membranes [27]. This technique works on the principle that ions diffuse from a high to low concentration; it uses ionic activity measurement taken at various positions in

the diffusion boundary layer to estimate the next flux of ions into the tissue, plant, or any other target sample [28,29]. To convert the gathered data, the following assumptions will need to be taken into consideration: 1) mechanism of ion transport, 2) nature of the diffusion boundary layer and 3) the geometry of target sample. Each assumption would yield different flux estimates for the same data. Furthermore, the flux and concentration gradients can be further divided in terms of radial or planar diffusion. In radial diffusion, the flux is inversely proportional to the radial distance, which is opposite to planar diffusion, where the area over which the flux occurs remains constant along the path of diffusing ions. For this study, planar diffusion has been studied to be the major source of EMF for plant tissues [28,29], therefore Fick's law was applied (Eq. 3).

$$J = D\frac{dc}{dx} \tag{3}$$

Where J represents the diffusion flux (mol m^{-2} s^{-1}), D (m^2/s) is the diffusion coefficient of the target ion under analysis, c is the concentration, x represents position. Figure 5 shows a schematic representation of MIFE analysis.

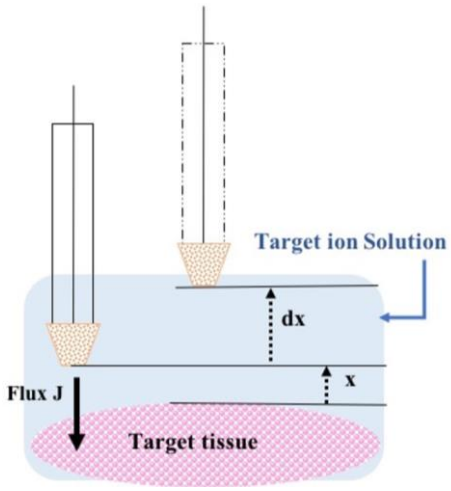

Figure 5. Schematic representation of microelectrode flux estimation applied to a target sample

1.7 References

[1] Bakker, E.; Pretsch, E. TrAC Trends in Analytical Chemistry 2001, 20, 11-19.
[2] Ceresa, A.; Bakker, E.; Hattendorf, B.; Gunther, D.; Pretsch, E. Analytical Chemistry 2001, 73, 343-351.
[3] Bühlmann, P.; Chen, L. D. In Supramolecular Chemistry; John Wiley & Sons, Ltd, 2012.
[4] Chumbimuni-Torres, K. Y.; Rubinova, N.; Radu, A.; Kubota, L. T.; Bakker, E. Analytical Chemistry 2006, 78, 1318-1322.
[5] Birinci, A.; Eren, H.; Coldur, F.; Coskun, E.; Andac, M. Journal of Food and Drug Analysis 2016, 24, 485-492.
[6] Fouskaki, M.; Chaniotakis, N. A. Analytical Chemistry 2005, 77, 1780-1784.
[7] Dagraca, J. V. Annual Review of Phytopathology 1991, 29, 109-136.
[8] Xia, Y.; Ouyang, G.; Sequeira, R. A.; Takeuchi, Y.; Baez, I.; Chen, J. Plant Health Progress 2011.
[9] Bakker, E.; Bühlmann, P.; Pretsch, E. Chemical Reviews 1997, 97, 3083-3132.
[10] Lazo Fraga, A. R.; Calvo Quintana, J.; Li Destri, G.; Giamblanco, N.; Toro, R. G.; Punzo, F. Journal of Solid State Electrochemistry 2012, 16, 901-909.
[11] Michalska, A.; Pyrzyńska, K.; Maksymiuk, K. Analytical Chemistry 2008, 80, 3921-3924
[12] Veder, J.-P.; De Marco, R.; Clarke, G.; Chester, R.; Nelson, A.; Prince, K.; Pretsch, E.; Bakker, E. Analytical chemistry 2008, 80, 6731-6740.
[13] Hu, J. B.; Stein, A.; Buhlmann, P. Trac-Trends in Analytical Chemistry 2016, 76, 102-114.
[14] Si, P. C.; Bakker, E. Chemical Communications 2009, 5260-5262.
[15] Veder, J. P.; De Marco, R.; Patel, K.; Si, P. C.; Grygolowicz-Pawlak, E.; James, M.; Alam, M. T.; Sohail, M.; Lee, J.; Pretsch, E.; Bakkert, E. Analytical Chemistry 2013, 85, 10495- 10502.
[16] Jaworska, E.; Mazur, M.; Maksymiuk, K.; Michalska, A. Analytical Chemistry 2018, 90, 2625-2630.
[17] Kim, Y.; Amemiya, S. Analytical Chemistry 2008, 80, 6056-6065.
[18] Crespo, G. A.; Macho, S.; Bobacka, J.; Rius, F. X. Analytical Chemistry 2009, 81, 676-681.
[19] Mathison, S.; Bakker, E. Analytical Chemistry 1998, 70, 303-309.
[20] Lai, C. Z.; Joyer, M. M.; Fierke, M. A.; Petkovich, N. D.; Stein, A.; Buhlmann, P. Journal of Solid State Electrochemistry 2009, 13, 123-128.
[21] Malon, A.; Radu, A.; Qin, W.; Qin, Y.; Ceresa, A.; Maj-Zurawska, M.; Bakker, E.; Pretsch,
[22] E. Analytical Chemistry 2003, 75, 3865-3871.
[23] Mensah, S. T.; Gonzalez, Y.; Calvo-Marzal, P.; Chumbimuni-Torres, K. Y. Analytical Chemistry 2014, 86, 7269-7273.
[24] Flores, S. C.; Kherb, J.; Konelick, N.; Chen, X.; Cremer, P. S. Journal of Physical Chemistry C 2012, 116, 5730-5734.
[25] Kunz, W.; Neueder, R. In Specific Ion Effects, Werner, K., Ed.; World Scientific: Germany, 2009, pp 3-7.
[26] Umezawa, Y.; Buhlmann, P.; Umezawa, K.; Tohda, K.; Amemiya, S. Pure and Applied

Chemistry 2000, 72, 1851-2082.
[27] Bakker, E. Analytical Chemistry 1997, 69, 1061-1069.
[28] Henriksen, G. H.; Raman, D. R.; Walker, L. P.; Spanswick, R. M. Plant Physiology 1992, 99, 734-747.
[29] Newman, I. A.; Kochian, L. V.; Grusak, M. A.; Lucas, W. J. Plant Physiology 1987, 84, 1177-1184.
[30] Newman, I. A. Plant Cell and Environment 2001, 24, 1

CHAPTER TWO: READY-TO-USE SINGLE-STRIP PAPER BASED SENSOR FOR MULTIPLEX ION DETECTION

Adapted with permission from Armas, S.M., Manhan, A.J., Younce, O., Chumbimuni-Torres, K.Y. Ready-to-use single-strip paper-based sensor for multiplex ion detection. Sens Actuators, B. 2017. 255, 1781-1787.

2.1 Introduction

With increasing demand for portable devices, paper-based sensors have become highly attractive due to their thin, lightweight, low-cost and flexible nature [1]. Since paper is made up of cellulose fibers and various pore sizes are largely available, a wide array of applications are accessible [1]. The versatility of paper-based sensors can be augmented by integrating them with ion-selective electrodes (ISEs), specifically polymer-based ISEs, as an analytical platform for ion detection. ISEs have gained momentum as an analysis tool, due to their versatility, high sensitivity and selectivity for ion detection in situ [2,3]. Therefore, paper-based solid-contact ISEs (PBSC-ISEs) are the ideal candidate for fieldwork applications, including environmental [2], biological [4] and food analysis [5]. A polymer-based ISE is composed of an ionophore, to render selectivity to the membrane by forming a stable complex with the analyte of interest; an ion-exchanger, to provide electroneutrality and ensure perm selectivity; and a polymer matrix to provide the support and mechanical functionality to the membrane. The ISEs response is dictated by the phase boundary potential (E_{PB}) (Eq.4) wherein a_I (aq) and a_I (org) are the activities of the primary ion (I^{z+}) of charge z in aqueous and organic phases, respectively. Furthermore, E°, R, T, and F are the

standard-potential, universal gas constant, absolute temperature, and Faraday constant, respectively [6].

$$E_{PB} = E^{0\prime} + \frac{RT}{z_I F} ln \frac{a_{I(aq)}}{a_{I(org)}} \quad (4)$$

In order to exhibit a Nernstian response, the activity of the primary ions in the bulk of the organic phase must remain constant and independent of the sample. Therefore, the E_{PB} can be reduced to the well-established Nernst Equation (Eq.5)

$$E_{PB} = E^{0\prime} + \frac{RT}{z_I F} \ln a_{I(aq)} \quad (5)$$

Furthermore, the ISE must be exposed to the primary ion of interest, to allow the ionophore to chelate the primary ion. This process has been regarded as the conditioning protocols of ISEs. For decades, traditional conditioning protocols have involved exposing the ISE to a high concentration of the ion of interest, a process that can take between 12–72 h [7]. For a cation-selective membrane, the established equilibrium process can be represented by the equation below:

$$I_{aq}^{z+} + nL_{org} + M_{org}^{+} R_{org}^{-} \leftrightharpoons [IL_n]_{org}^{z+} + M_{aq}^{+} + R_{org}^{-} \quad (6)$$

Where, L is the ligand that forms the ion-ionophore complex with primary ion I^{z+}, with stoichiometry n. $M_{org}^{+} R_{org}^{-}$is the ion-exchanger, composed of a lipophilic anion R^{-} and a cation M^{+}. The cation will partition to the aqueous phase and exchange with the primary ion I^{z+}. The lipophilic anion will remain in the membrane to retain electroneutrality and allow permselectivity [6]. This lengthy protocol prevents practical and efficient applications of these sensors. Therefore, new efforts in creating a condition-free ISE are required. Recently, the Buhlmann group used non-conditioned ISEs in a paper substrate. However, a liquid-junction

platform was used for both the ISE and RE, and a new sensor must be used for each point of a calibration curve [8]. Herein, to circumvent the conditioning step, addition of the ion of interest directly into the membrane cocktail was done as described in Rich et al. [6] and was optimized for its integration to a PBSC platform. Consequently, the primary ion, I^{z+} is already present in the membrane and is able to form the ion-ionophore complex according to the equilibrium below:

$$I_{org}^{z+} + nL_{org} + R_{org}^{-} \leftrightharpoons [IL_n]_{org}^{z+} + R_{org}^{-} \quad (7)$$

In order to conduct potentiometric measurements, the PBSC-ISE must work in conjunction with a reference electrode. Commonly used reference electrodes are bulky and fragile, preventing their use for in-field applications. In order to overcome this limitation, recent research has proposed various methods to develop an alternative reference electrode that are insensitive to changes in electrolyte concentration [9]. Some approaches include references electrodes based on polyurethanes, silicon rubber, polyvinyl chloride and acrylate membrane, yet all of these approaches require soaking the reference electrode in electrolyte solution prior to use [10–13]. In addition, various lipophilic additives such as ETH 500 [14] and ionic liquids (ILs) [15–17] were proposed. From these methods, employing ILs, appeared to be the most promising option as the phase boundary potential of the reference electrode is defined by slow partitioning of the IL to the aqueous phase [16,18]. Therefore, ILs are excellent candidates towards a stable reference electrode. It is crucial to assure equipartition of the IL to the aqueous phase in order to avoid ion exchange effects. If an ion of the IL exchanges with an ion of the bulk solution of equal charge, the membrane will render a response to that ion and thus will be unable to function as a reference electrode [15]. Previous research showed that 1-Ethyl-3-methylimidazolium bis(trifluoromethane sulfonyl)amide $[C_2mim]^+$ $[NTF_2]^-$ was the most suitable IL to be used for the development of a

reference electrode [15]. Its response in a PVC/IL membrane exhibited a potential change of less than 10 mV for a variety of ions, including, Li^+, Na^+, K^+, Pb^{2+}, over a wide concentration range after conditioning in 1×10^{-3}M KCl solution. Lastly, $[C_2mim]^+$ $[NTF_2]^-$ based reference electrodes exhibit a great working pH range of 2.7–11.4. The effectiveness of $[C_2mim]^+$ $[NTF2]^-$ is likely due to similar mobility of the anion with respect to the cation based on Hildebrand's solubility parameters [19]. Therefore, we propose to develop a sensor that incorporates a PBSC-ISE and a paper-based solid-contact reference electrode (PBSC-RE), integrated in a single-strip style for multiplex analysis, and which does not require a conditioning step, see Fig. 2A-1 In this work, the PBSC-RE will incorporate the copolymer methyl methacrylate-co-decyl methacrylate (MMA-DMA) (support matrix), combined with the $[C_2mim]^+$ $[NTF_2]^-$ IL to create and maintain a stable potential that is unaffected by an increase in ionic activity and will not require a conditioning step. The chosen matrix (MMA-DMA) does not require the use of a plasticizer, resulting in an extended lifetime. The proposed system could potentially be used to monitor Na^+, K^+ and I^- levels in vitro. In turn, aiding in early prognosis of hyponatremia, hypokalemia and iodine deficiency which can lead to goiter, prior to reaching a critical state. A ready-to-use PBSC-ISE sensing platform would not need highly trained personnel to implement traditional conditioning protocols. The PBSC-ISE platform would also enable cost-effective on-site analysis, and its intrinsic flexibility due to a paper-based substrate, would increase durability and lower risk of damage to the sensor due to mishandling.

2.2 Experimental Section

Reagents and Materials. 4-tertbutylcalix[4]arene-tetracetic acid tetraethyl ester (sodium ionophore X, NaIX), sodium tetrakis [3,5-bis-(trifluoromethyl)phenyl]borate (NaTFPB),

valinomycin (potassium ionophore I), potassium tetrakis [3,5-bis-(trifluoromethyl)phenyl]borate (KTFPB), bis-(2-ethylhexylsebacate) (DOS), tridodecylmethylammonium nitrate (TDMANO3), all Selectophore grade, were obtained from Sigma-Aldrich (Milwaukee, WI). [9]-Mercuracarborand-3 (MC3) was synthesized in-house [20] as previously described. Potassium chloride (KCl), sodium chloride (NaCl), calcium chloride dihydrate ($CaCl_2 \cdot 2H_2O$), lithium chloride (LiCl), potassium iodide (KI), sodium iodide (NaI) and sodium nitrate ($NaNO_3$) ACS reagent, ≥99.0%, poly-(3-octylthiophene-2,5-diyl) (POT) and 2, 2′ azo-bis(isobutyronitrile) (AIBN, 98% purity), high molecular weight polyvinyl chloride (PVC) and tetrahydrofuran were all obtained from Sigma-Aldrich (Milwaukee, WI). Methyl methacrylate (99.5% purity) and n-decyl methacrylate (99% purity) were obtained from Polysciences (Warrington, PA). Single-walled carbon nanotubes(SWCNTs) of 99% purity were obtained from Cheap Tubes Inc (Grafton, VT). The methyl methacrylate-co-decyl methacrylate (MMA:DMA; 42:58) copolymer was synthesized in house following procedure in Qin et al. [21] and characterized as in Mensah, et al.[22] Methylene chloride, chloroform, ethyl acetate, 1,4-dioxane, and qualitative filter paper (Whatman catalog no. 1001090) were obtained from Fisher (FairLawn, NJ). 1-Ethyl-3-methylimidazolium$[C_2mim]^+$Bis(trifluoromethane sulfonyl)amide $[NTF_2]^-$ IL was acquired from Strem Chemicals Inc (Newburyport, MA). All solutions were prepared using deionized water purified by a Millipore Milli-Q (Billerica, MA).

2.2.1 Preparation of Paper-Based Substrate

The paper-based substrates were developed as described in Mensah et al. [20] Briefly, a 3.0 mg/mL SWCNT suspension was prepared and coated onto a 6.5 cm × 5.5 cm qualitative filter paper with a conventional paintbrush. Six coats were applied and allowed to dry at room

temperature for 10 min, followed by 20 min in an oven at 60 C, after each coating. The conductivity was measured using a source measurement unit (Keithley Source-Meter model 2400, Cleveland, OH). At the bottom of each filter paper sheet, a 0.5 cm diameter orifice was exposed and sputtered with gold (Denton Vacuum LLC Desk IV, Moorestown, NJ). At the gold sputtered point, 60 μL of a 25mM (with respect to the monomer) solution of POT dissolved in methylene chloride (DCM) was drop-casted, 10μL at a time, at 5 min intervals. The POT was allowed to dry overnight. The filter paper SWCNT substrate was then cut into 1.0 cm ×5.5 cm strips and each sensor were partially covered in a mask of non-permeable D-Wrap Blue PolyesterTape.

2.2.2 Preparation of Condition-Free PBSC

Na^+, K^+, and I^- ISEs. The Na^+ cocktail was prepared by adding 5 mmol/kg of NaTFPB, 10 mmol/kg of NaIX, (66.6 w%) DOS and (33.3 w%) PVC, dissolved in 1 mL of THF and vortexed for 1 h. The K^+ cocktail was composed of 5 mmol/kg of KTFPB, 10 mmol/kg of potassium ionophore I, (66.6 w%) DOS and (33.3 w%) PVC. The I^- cocktail contained 1.0 mmol/kg of MC3, 0.75 mmol/kg of $TDMANO_3$ and 1.8 μL of 0.1 M NaI aqueous solution to circumvent the conditioning step in a total mass of 240 mg. Control membranes were also prepared following the composition as described in Rich et al. Briefly, sodium and potassium control membranes replaced the ion exchanger to KTFPB and NaTFPB, respectively. In the case of the iodide control membrane, no NaI solution was added. However, the effect of hydration of the membrane upon addition of an aqueous solution was considered, and 1.8 μL of H_2O was added to the control membrane. Three 12.5 μL aliquots of the cocktail was drop-casted onto the POT coated paper SWCNT substrate. These were allowed to dry overnight prior to measurement. The

thickness of the membrane film was obtained using a caliper. The average thickness was found to be 193 ± 54 μm.

2.2.3 Preparation of PBSCs

40 mg of MMA:DMA and 40 mg of IL were dissolved in 1 mL of DCM and vortexed for ~30 min or until dissolved. The membrane cocktail was drop casted under a DCM environment, and an ice bath was used to lower the temperature of the system to prevent abrupt evaporation of the solvent. This prevented the formation of air bubbles, allowing for a uniform, clear film. A total of 90 μL was drop-casted onto the POT coated paper SWCNT substrate. Various ratios of MMA:DMA to IL was investigated and will be further discussed.

2.2.4 EMF Measurements

Potentials were monitored with a high-input impedance ($10^{15}\Omega$) EMF-16 multichannel data acquisition system (Precision Eletrochemistry EMF Interface, Lawson Laboratories, Malvern, PA) at room temperature (22°C), while stirring the solution. The condition-free Na^+, K^+, and I^- ISEs, as well as the PBSC-REs were tested against a double junction Ag/AgCl/3MKCl/1MLiOAc reference electrode (Metrohm AG). Aliquots of NaCl, KCl and NaI were respectively added at 10 min intervals. All electrodes were stored under ambient conditions and measurements were done in triplicates.

2.3. Results and Discussion

A previous study proposed to employ two commercially available ion-exchangers, KTFPB and NaTFPB for the development of a potassium ISE with shorter conditioning times [23]. Nevertheless, reported methods still require a minimum conditioning time of 3–5 h, depending on the analyte [23]. We have optimized this protocol to develop a condition free solid-contact ISE

on a paper substrate platform. This work allows the ability to choose between two systems: if a commercially-available ion-exchanger containing the ion of interest is available, it can be included to the sensing cocktail directly; or if it is not commercially available, a calculated aqueous aliquot of the ion of interest can be added to the cocktail composition to circumvent the conditioning step. In this study, a PVC/DOS matrix was used due to its characteristically faster ion diffusion coefficients, D, on the order of 10^{-8}cm^2/s in comparison to a diffusion coefficient on the order of 10^{-11} cm^2/s for poly(n-butylacrylate) based membranes [23]. This enables faster hydration of the membrane, facilitating ion partitioning between the organic and aqueous phase. In order to calculate the amount of ionic additive to be added, the ionophore to ion stoichiometric binding complexes were examined [24] and adjusted accordingly to allow the ionophore and respective ionic sites to buffer the primary ion of interest during sensing [25]. Figure 6 shows the potential response over time of a sodium, potassium and iodide ISE and their respective calibration curve plotted as a function of potential vs logarithm of activity of the ion of interest. The Na^+-ISE yielded an average Nernstian Response of 56.55 ± 0.79 mV decade^{-1} with a limit of detection (LOD) in the order of 5.6 ± 0.5 × 10^{-7} M (Fig. 6A). The K^+-ISE yielded an average Nernstian response of 57.82 ± 0.37 mV decade^{-1} with an LOD of 1.2 ± 0.2 × 10^{-7} M (Fig. 6B). The I^--ISEs yielded an average Nernstian response of −61.46 ± 1.24 mV with a LOD of 1.5 ± 0.6 × 10^{-7} M (Fig. 6C). All responses are comparable to those obtained when subjecting the ISEs to the conditioning protocol [26–28]. Control membranes were prepared without adding the primary ion into the cocktail, nor exposing it to its primary ion solution. Fig. 6D–F, show a super-Nernstian response for Na^+, K^+, and I^- ions respectively, due to a flux of primary ions from the sample solution into the bulk of the membrane, as a result of an uncomplexed ionophore. It is

worthwhile to highlight that all non-conditioned membranes require an initial hydration time of at least 20 min in order to have a drift of less than 1 mV/h.

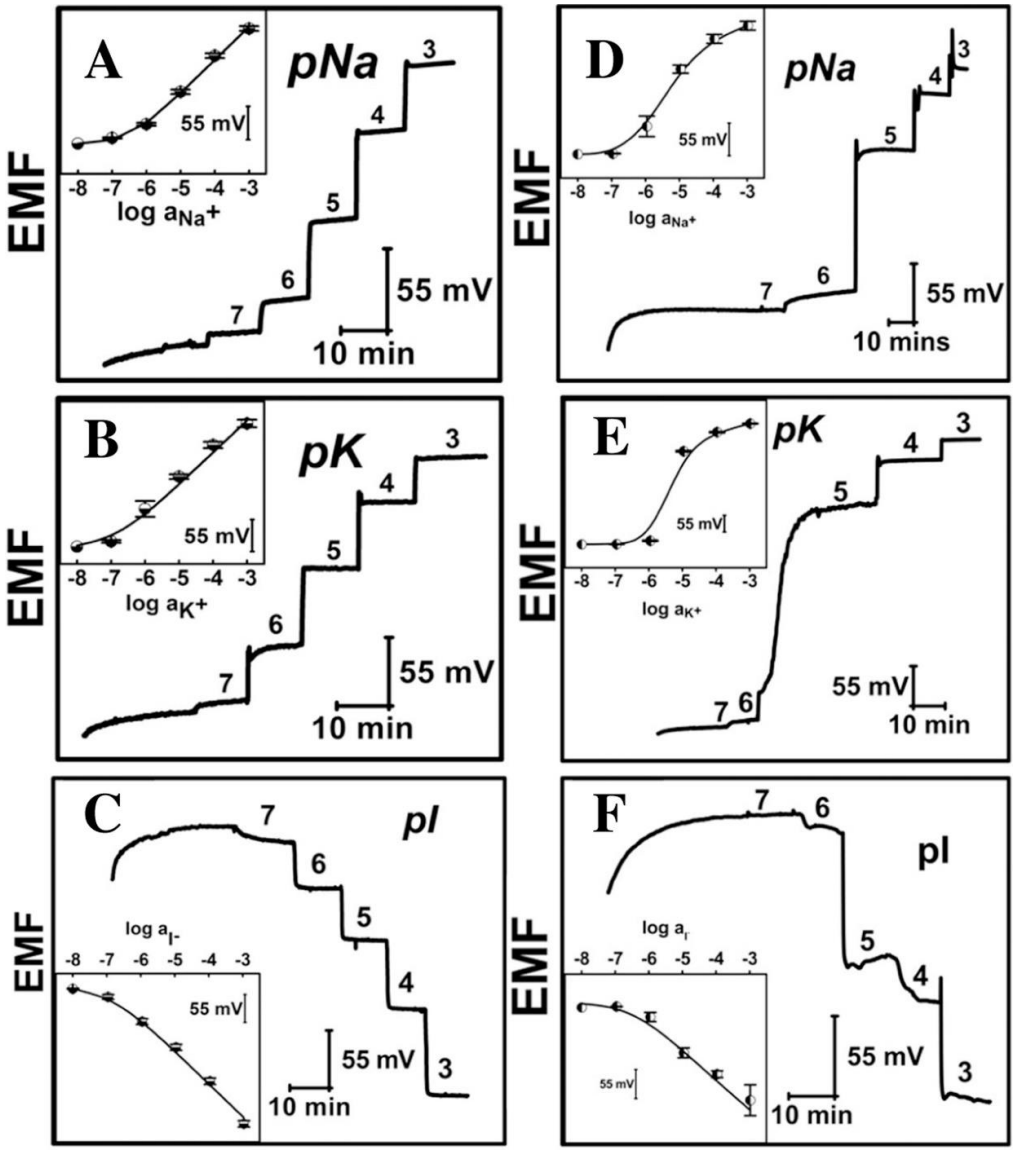

Figure 6. Potentiometric response obtained from condition-free Na^+ISE containing NaTFPB (A), containing KTFPB (D); K^+ ISE containing (B), containing NaTFPB (E); I^- ISE with addition of 1.8µL of NaI in the cocktail (C); no analyte added, 1.8µL of water in the cocktail (F). All measurements were performed against double junction Ag/AgCl/3MKCl/1MLiOAc

Furthermore, the K^+-ISE was exposed to increasing and decreasing concentrations of 10^{-5}, 10^{-4}, 10^{-3} M KCl. Overall, the potential response was fast and reproducible, demonstrating the reversibility of the sensor (Fig. 7).

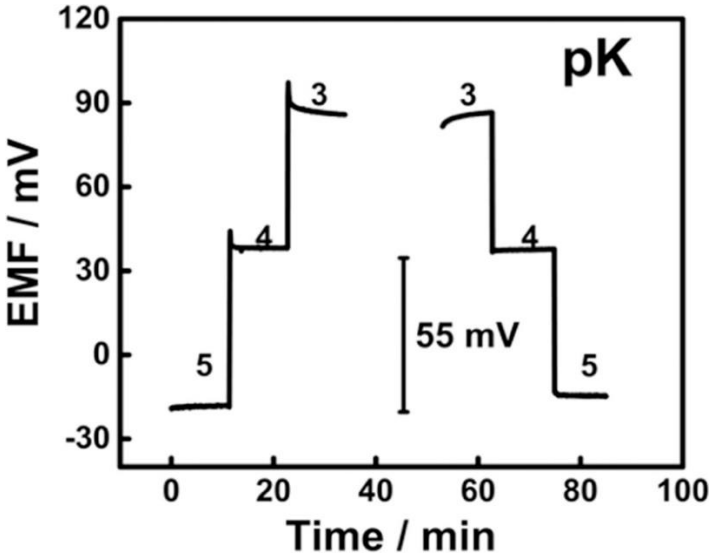

Figure 7. Potential reproducibility of K^+ ISE

Research in reference electrode development employing ILs has commonly used PVC [15,17]. However, PVC is known to have anionic impurities [21], which it was initially sought as a starting system towards reference electrode development. However, in this work PVC based membranes led to a potential drift of ~16 mV/h in water, as thus further experiments using a PVC matrix were no longer pursued. Consequently, MMA-DMA was used instead of PVC to alleviate this challenge. An ideal reference electrode should exhibit very small changes in potential across a wide range of concentrations [13]. Here, various ratios of ILs%: MMA-DMA% were investigated, including: 33.3: 66.6, 25: 75, and 50: 50. The composition with 33.3% IL exhibited a response greater than 15 mV at 1×10^{-3} M NaCl or KCl, so it was discarded as a suitable reference. The 25:75 PBSC-RE cocktail did not reach equilibrium as readily as the other compositions and

exhibited a very high resistance upon initial addition of electrolyte to the water background. In addition, the limited availability of the IL in the 25: 75 compositions prevented the IL to dictate and maintain a stable the phase boundary potential. The 50:50 ratio led to the least potential change over a range from 10^{-7} to 10^{-3} M of NaCl or KCl or NaI solutions with a respective response of 1.83 ± 2.75 mV response upon NaCl additions, 0.86 ± 0.44 mV response upon KCl additions and 2.03 ± 2.75 mV response upon exposure to NaI additions (Fig. 2.A-3). As a result, composition employing 50:50 (IL: MMA-DMA) was utilized for further experiments and integration with the ISE. Furthermore, the thickness of the membrane also plays an important role in the ideal response of the reference electrode, as increasing the membrane thickness reduces permeation of ions. This is important because it is hypothesized that a thinner membrane does not yield a well-defined reference potential, likely due to the fact that the organic phase is so thin, it is unable to create a proper phase boundary potential as dictated by IL partitioning, and thus is not able to serve as a reference electrode. Therefore, the thickness of the membrane was adjusted to 167 ± 15 μm. Additionally, much like the non-conditioned ISE membranes, the reference electrode also requires a hydration time of at least 20 min to yield a desired drift of less than 1 mV/h, similar for commercial reference electrodes, see Fig. 2.A-2 in the supporting information.

2.3.1 PBSC-RE pH Studies

Since the proposed sensors are designed for monitoring ionic activities in biological systems, it was essential to determine their working pH range. Therefore, the response to a change in pH was evaluated for the optimal composition of the reference electrode and the measurement was conducted in a triplicate manner. The experiment was performed in 100 mL of water using

solutions of HCl and NaOH to gradually change the pH from 3.11 to 12.11. The greatest potential difference was noticed at low and high pH (>5mV). The PBSC-RE presents a great working range of pH 5 to pH 10 with only a potential difference of only 0.25 ± 0.06 mV, which is applicable to most biological [29] and environmental samples [30]. Once again, the ideal response should be less than 1mV change across the abovementioned range. Fig.8 demonstrates that the reference electrodes exhibit an ideal working range between pH 5 and pH 10, with only a 0.25 ± 0.06 mV potential change.

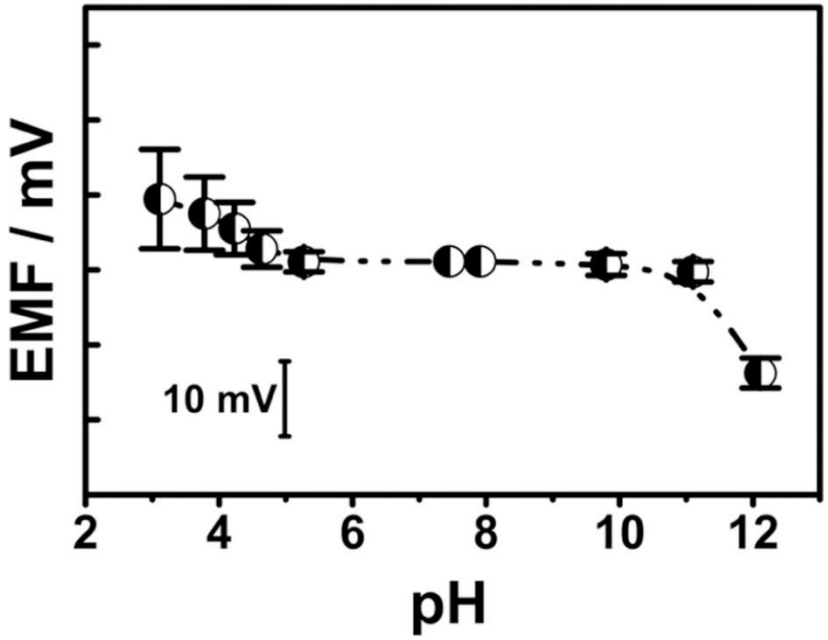

Figure 8. Potentiometric responses of PBSC-RE against commercial double-junction Ag/AgCl/3MKCl/1MLiOAc reference electrode

2.3.2 Water Layer Test

It is known that solid-contact electrodes often suffer from the formation of a thin aqueous layer in between the polymeric membrane and solid substrate, because of slow water diffusion and lack of a well-defined redox couple at the membrane-metal interface [31]. This membrane metal interface can create an aqueous reservoir that would house ionic entities that may lead to poor

limits of detection [31]. For this reason, a self-assembled monolayer of POT is applied between the gold layer and the polymeric membrane.

Here, no negative drift was noticed when changing the solution to the interfering ion solution (Fig. 9). In theory, if a water layer has formed, a positive drift is seen upon exposure to a solution containing a discriminating ion, followed by a negative drift upon re-exposure to solution containing the primary ion [32]. Nevertheless, the potential when electrodes were exposed to 1×10^{-3}M LiCl, remained stable even after 4 h and no negative drift was observed upon exposure to primary ion solution, 1×10^{-3} M NaCl. Consequently, it is hypothesized that no water layer was formed.

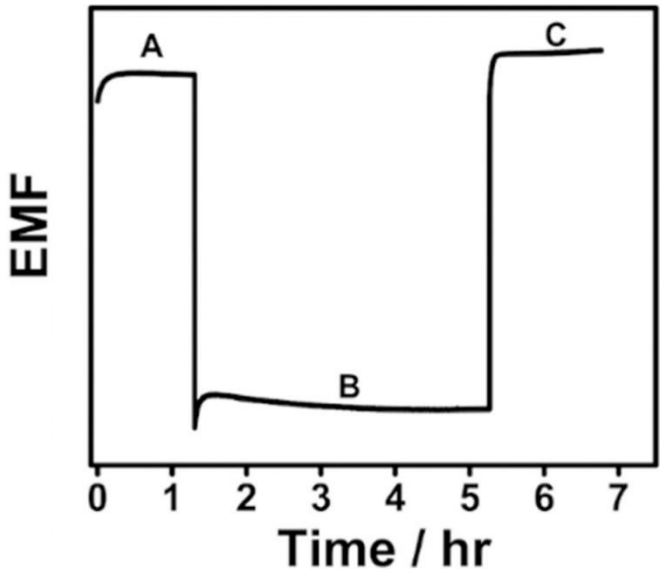

Figure 9. Water Layer Test for Condition free PBSC Na^+ISEs. At time t=1.3h primary ion solution $1x10^{-3}$M NaCl (A) was exchanged for $1x10^{-3}$M LiCl (B). At 5.3h the sample solution was replaced to primary ion $1x10^{-3}$M NaCl (C) until t=6.6h.

2.3.3. Integrating Condition-Free PBSC-ISE to PBSC-RE

Once the conditioning step was circumvented, and the reference membrane composition and preparation protocol were optimized; the two electrodes were integrated into a single-strip style

sensor. This yielded a Nernstian response of 54.85 ± 0.28 mV decade^{-1} with an LOD of 9.7 ± 0.1 × 10^{-7} M for K^+-ISEs (Fig.10A) and a −52.98 ± 0.85 mV decade^{-1} with an LOD of 2.6 ± 0.9 × 10^{-7}M (Fig. 10B) for I^- ISEs. The LOD of the self-referenced condition-free electrodes are comparable to those obtained using the double junction reference electrode. Therefore, these sensors could potentially be utilized for in situ analysis using a portable potentiometer.

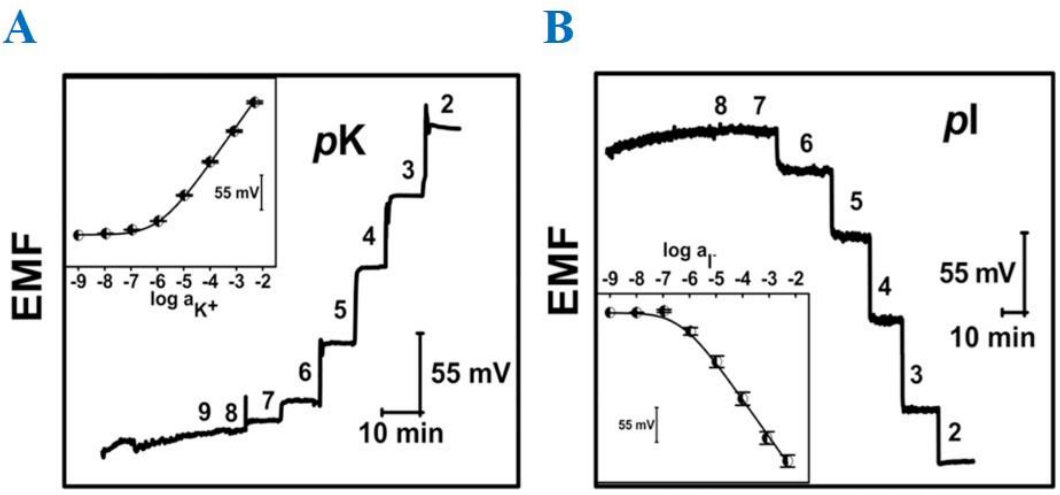

Figure 10. Potentiometric response for single-strip condition-free PBSC A) Potassium and B) Iodide ISEs

2.3.4. Flexibility Study of PBSC-RE and PBSC-ISEs

Today, there is a high demand for cost-effective and reliable point-of-care devices that can be employed in a low-income and underdeveloped health systems, or for home-based testing [33]. Therefore, the flexibility of the device is important when utilized by non-trained personnel to avoid risk of damage to the device. Here, flexibility studies were done to both, the PBSC-RE and PBSC-ISE to test the feasibility of the complete platform. Each electrode was folded forward (held pressure for ~1 min and release) and backward (held pressure for ~1 min and release) twice in a manner represented by Fig. 11B. The applied stress was done at two points of the sensors as seen in Fig. 11A at ‘applied stress 1′ and ‘applied stress 2′.

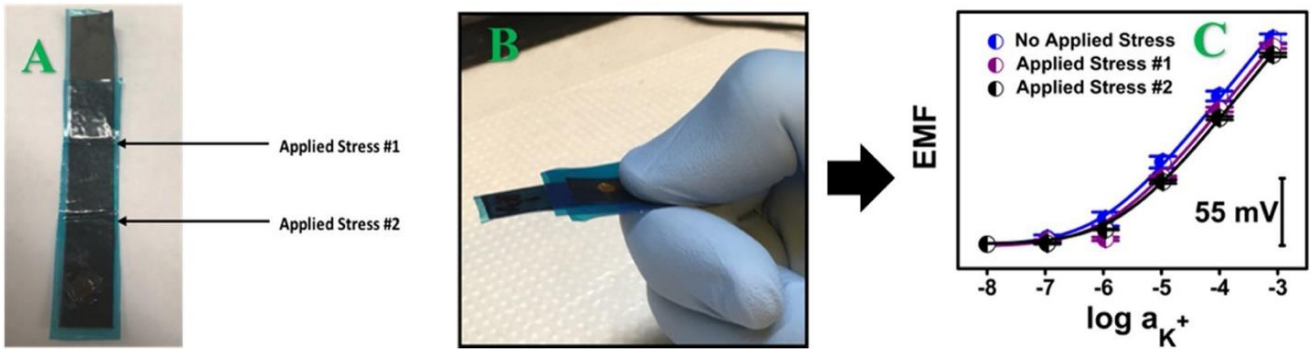

Figure 11. A) Paper-Based Electrode after first and second applied stress; B) demonstration of applied stress. C) Calibration curves of K^+ ISE response before applied stress (blue), after applied stress #1 (purple), after applied stress #2 (black).

The electrodes response was measured before and after each stress was applied. The response of the electrodes was 53.33 ± 1.20 mV with an LOD of 8.57 ±1.26 × 10^{-7} M without any applied stress (Fig.11C blue); 56.58 ± 1.20 mV with an LOD of 1.56 ± 0.06 × 10^{-6} M after 'applied stress #1′ (Fig.11C purple), and 54.78 ± 0.09 mV with an LOD of 1.33 ± 0.09 × 10^{-6} M (Fig.11C black) after 'applied stress #2′. Overall, the PBSC-ISEs platform response remain the same upon applied stress.

2.3.5. Multiplex Detection of K^+ and I^- Ions in Water Background Employing Single-Strip Condition-Free PBSC-RE

A time-efficient way to analyze blood or environmental samples is to target multiple ions simultaneously. Here, standards of potassium iodide were prepared to test the proposed platform for simultaneous detection of K^+ and I^- ions. Results yielded a slope of 53.25 ± 1.23 mV for K^+ and −56.20 ± 0.2 mV for I^- with a respective LOD of 5.7 ± 1.7 × 10^{-7} M and 6.8 ± 0.3 × 10^{-7} M (Fig. 12).

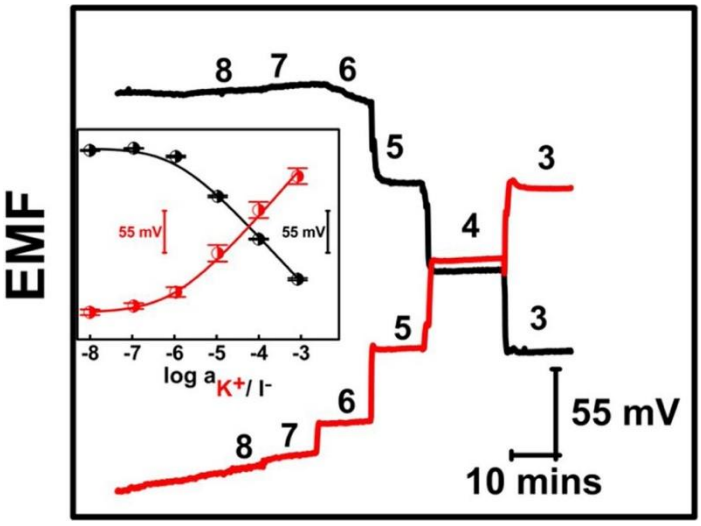

Figure 12. Multiplex detection of K+ and I- ions in water background employing single-strip condition-free PBSC-ISE

2.3.6. Selectivity Measurements

Selectivity measurements for K^+, and I^- ISEs' were obtained using the separate solutions method as described by Bakker [34]. The slopes and selectivity coefficients are displayed in Table 1. It should be noted that some of the interfering ions response are still sub-Nernstian, indicating bias to some extent, hence the slight difference in selectivity coefficients, yet they are still within the range necessary for practical use. Nevertheless, it is within the range reported in literature [6,28,35].

Table 1. Observed selectivity coefficients for K^+ ISEs and I^- ISEs with corresponding slope for interfering ions based on the separate solutions methods.

Ion $J^{(z+)}$	$K_{K,J}^{pot}$	**Slope (mV decade^{-1})**
Ca^{2+}	-5.26 ± 0.10	18.89 ± 1.05
Li^+	-3.37±0.37	11.50 ± 1.94
Na^+	-2.00±0.24	21.86±2.24
K^+	0	57.91±0.69

Ion $J^{(z+)}$	$K_{I,J}^{pot}$	Slope (mV decade^{-1})
Cl^-	-2.82±0.06	-61.58 ± 2.82
NO_3^-	-4.22±0.2	-26.20±0.45
I^-	0	-59.66 ± 2.14

2.4 Conclusions

Herein, a ready-to-use single-strip PBSC-ISE platform for multiplex ion analysis has been developed. The ready-to-use feature was possible by circumventing lengthy conditioning protocols, via simple addition of primary ions upon preparation of the sensing cocktail. The PBSC platform was designed to be operated without the need for specialized trained personnel. Users will be able to utilize the sensors without the risk damaging the response of the sensor upon external stress. The intrinsic nature of the paper leads to a cost-effective sensor with an overall cost of the multiplex platform estimated to be ~$0.96 per sensor, a cost difficult to achieve with biodegradable plastics, which are more expensive. This single-strip ready-to-use sensor could potentially be used to monitor for imbalances of sodium (Na^+), potassium (K^+) and iodide (I^-) in blood, sweat, or other bodily fluids. Monitoring levels of these ions can be crucial indicators to human health.

2.5. References

[1] Liana, D. D.; Raguse, B.; Gooding, J. J.; Chow, E. *Sensors* **2012**, *12*, 11505.
[2] Fucskó, J.; Tóth, K.; Pungor, E.; Kunovits, J.; Puxbaum, H. *Analytica Chimica Acta* **1987**, *194*, 163-170.
[3] Novell, M.; Guinovart, T.; Blondeau, P.; Rius, F. X.; Andrade, F. J. *Lab on a Chip* **2014**, *14*, 1308-1314.
[4] van de Velde, L.; d'Angremont, E.; Olthuis, W. *Talanta*.
[5] Nery, E. W.; Kubota, L. T. *Analytica Chimica Acta* **2016**, *918*, 60-68.

[6] Rich, M.; Mendecki, L.; Mensah, S.; Blanco-Martinez, E.; Armas, S.; Calvo-Marzal, P.; Radu, A.; Chumbimuni-Torres, K. *Analytical Chemistry* **2016**, *88*, 8404-8408.
[7] Lazo Fraga, A. R.; Calvo Quintana, J.; Li Destri, G.; Giamblanco, N.; Toro, R. G.; Punzo, F. *Journal of Solid State Electrochemistry* **2012**, *16*, 901-909.
[8] Hu, J. B.; Stein, A.; Buhlmann, P. *Angewandte Chemie-International Edition* **2016**, *55*, 7544-7547.
[9] Chen, C. C.; Chou, J. C. *Japanese Journal of Applied Physics* **2009**, *48*.
[10] Bakker, E. *Analytical Chemistry* **2016**, *88*, 395-413.
[11] Guinovart, T.; Crespo, G. A.; Rius, F. X.; Andrade, F. J. *Analytica Chimica Acta* **2014**, *821*, 72-80.
[12] Rius-Ruiz, F. X.; Bejarano-Nosas, D.; Blondeau, P.; Riu, J.; Rius, F. X. *Analytical Chemistry* **2011**, *83*, 5783-5788.
[13] Bakker, E. *Electroanalysis* **1999**, *11*, 788-792.
[14] Mattinen, U.; Bobacka, J.; Lewenstam, A. *Electroanalysis* **2009**, *21*, 1955-1960.
[15] Cicmil, D.; Anastasova, S.; Kavanagh, A.; Diamond, D.; Mattinen, U.; Bobacka, J.; Lewenstam, A.; Radu, A. *Electroanalysis* **2011**, *23*, 1881-1890.
[16] Hu, J. B.; Ho, K. T.; Zou, X. U.; Smyrl, W. H.; Stein, A.; Buhlmann, P. *Analytical Chemistry* **2015**, *87*, 2981-2987.
[17] Zou, X. U.; Chen, L. D.; Lai, C.-Z.; Bühlmann, P. *Electroanalysis* **2015**, *27*, 602-608.
[18] Zhang, T.; Lai, C.-Z.; Fierke, M. A.; Stein, A.; Bühlmann, P. *Analytical Chemistry* **2012**, *84*, 7771-7778.
[19] Marciniak, A. *International Journal of Molecular Sciences* **2010**, *11*, 1973-1990.
[20] Zinn, A. A.; Zheng, Z. P.; Knobler, C. B.; Hawthorne, M. F. *Journal of the American Chemical Society* **1996**, *118*, 70-74.
[21] Qin, Y.; Peper, S.; Bakker, E. *Electroanalysis* **2002**, *14*, 1375-1381.
[22] Mensah, S. T.; Gonzalez, Y.; Calvo-Marzal, P.; Chumbimuni-Torres, K. Y. *Analytical Chemistry* **2014**, *86*, 7269-7273.
[23] Michalska, A.; Pyrzyńska, K.; Maksymiuk, K. *Analytical Chemistry* **2008**, *80*, 3921-3924.
[24] Bakker, E.; Bühlmann, P.; Pretsch, E. *Chemical Reviews* **1997**, *97*, 3083-3132.
[25] Bühlmann, P.; Chen, L. D. In *Supramolecular Chemistry*; John Wiley & Sons, Ltd, 2012.
[26] Novell, M.; Parrilla, M.; Crespo, G. A.; Rius, F. X.; Andrade, F. J. *Analytical Chemistry* **2012**, *84*, 4695-4702.
[27] Cadogan, A. M.; Diamond, D.; Smyth, M. R.; Deasy, M.; McKervey, M. A.; Harris, S. J. *Analyst* **1989**, *114*, 1551-1554.
[28] Malon, A.; Radu, A.; Qin, W.; Qin, Y.; Ceresa, A.; Maj-Zurawska, M.; Bakker, E.; Pretsch, E. *Analytical Chemistry* **2003**, *75*, 3865-3871.
[29] Ivan, M. G.; Wiegersma, S.; Sweelssen, J.; Saalmink, M.; Boersma, A.; Ieee. *2011 Ieee Sensors* **2011**, 292-295.
[30] Hijaz, F.; Killiny, N. *Plos One* **2014**, *9*, 11.
[31] Fibbioli, M.; Morf, W. E.; Badertscher, M.; Rooij, N. F. d.; Pretsch, E. *Electroanalysis* **2000**, *12*, 1286-1292.
[32] Hu, J. B.; Stein, A.; Buhlmann, P. *Trac-Trends in Analytical Chemistry* **2016**, *76*, 102-114.
[33] Pai, N. P.; Vadnais, C.; Denkinger, C.; Engel, N.; Pai, M. *Plos Medicine* **2012**, *9*, 7.
[34] Bakker, E. *Analytical Chemistry* **1997**, *69*, 1061-1069.

[35] Cosofret, V. V.; Erdosy, M.; Buck, R. P.; Kao, W. J.; Anderson, J. M.; Lindner, E.; Neuman, M. R. *Analyst* **1994**, *119*, 2283-2292.

CHAPTER THREE: DEVELOPMENT AND CHARACTERIZATION OF NEEDLE-TYPE ION-SELECTIVE MICROSENSORS FOR IN SITU DETERMINATION OF FOLIAR UPDATE OF ZN^{2+} IN CITRUS PLANTS

Adapted with permission from Church, J†., Armas, S.M†., Patel, P.K., Chumbimuni-Torres, K.Y., Lee, W.H. Development and characterization of needle-type ion-selective microsensors for in situ determination of foliar uptake of Zn^{2+} in citrus plants. Electroanalysis. 2017, 29, 1-8

3.1 Introduction

In the span of 10 years, Huanglongbing (HLB) has devastated Florida's 10.7-billion-dollar citrus industry. HLB has now spread into commercial groves and growers are struggling to maintain profits. Citrus HLB, or citrus greening, is caused by three species of Alphaproteobacteria: 1) Candidatus Liberibacter asiaticus (Ca. L. asiaticus (Las)), 2) Ca. L. africanus (Laf), and 3) Ca. L. americanus (Lam), which are limited to growth in the phloem [1]. The disease plugs the sieve pores of the phloem which ultimately inhibits the flow of nutrients throughout the tree [2]. Therefore, HLB symptoms hallmarks nutrient deficiency; blotchy mottle leaves, yellow shoots and fruits that are underdeveloped and lopsided [3]. Citrus trees infected with HLB have been shown to exhibit depleted levels of zinc when compared to healthy citrus trees [4]. A study has shown that zinc concentrations could be ten times greater in healthy trees [5]. Therefore, it has been common practice to supplement HLB infected trees with nutrients like zinc to alleviate the nutrient imbalance [6]. Nevertheless, it is still unclear on whether nutritional therapy can alleviate the symptoms of HLB. Additionally, there is limited research connecting nutritional management

to improved productivity of HLB infected citrus trees and recent reports have shown that nutritional therapy is not effective at suppressing Las or alleviating HLB symptoms [7]. The lack of information is likely due to current methodology employed to monitor zinc content in citrus plants. Currently, zinc is detected primarily using inductively coupled plasma atomic emission spectroscopy (ICP-AES) or atomic absorption spectroscopy (AAS) for which samples need to be dried, grounded, and digested before analysis [8]. This process is time consuming, expensive, destructive, non-portable and does not give the temporal or spatial resolution needed to truly understand the movement of zinc through the phloem of citrus plants. Therefore, there is an urgent need to develop a reliable, non-invasive, non-destructive tool capable of tracking zinc's systemic activity directly in plants.

Polymer-based micro ion-selective electrodes (µ-ISE) can meet the desired qualities of a non-invasive tool for in situ analysis of citrus plants. These µ-ISEs provide the needed selectivity via the use of an ionophore, which forms a stable complex with the analyte of interest; an ion-exchanger, which provides electroneutrality and ensures permselectivity; and a polymer matrix which yields high support and mechanical functionality to the membrane. Non-invasive microelectrode ion flux estimation (MIFE) has been used to study the transport of ions in plant physiology due to the non-destructiveness and high spatial and temporal resolution of the method in almost natural conditions. Works by Miller et.al [9] and Newman [10] have pioneered the practical and versatile use of microelectrodes and MIFE for plant studies. Ions including H^+, Ca^{2+}, NO_3^-, NH^{4+}, Na^+, Cl^-, Cd^{2+} and K^+ have been investigated using MIFE techniques [11]. Nonetheless, these studies did not perform foliar uptake of zinc via ion flux estimation due to the lack of appropriate analytical tools. Further, these previous studies have employed a liquid-

contact (LC) based platform for µ-ISEs [9a,10b,11]. However, the optimization and insertion of the backfilling solution can be laborious and challenging to yield lower limits of detection (LOD) and good electrode reproducibility. As a result, this work employs a solid-contact (SC) based platform to overcome the challenges from LC based platform. SC-µ-ISEs allow for less cumbersome LOD optimization due to its simplistic design. In a SC based platform, the ionophore-doped polymeric membrane is in direct contact with the metallic conductor (e.g., gold) coated with a hydrophobic conducting polymer (poly (3-octylthiophene- 2,5 diyl)), leading to an improved membrane/metal interface and a stable phase boundary potential, allowing trace level analysis [12]. The objective of the present work was to develop, characterize, and apply a zinc SC-µ-ISE for determining in situ foliar uptake of Zn^{2+} in citrus plants using MIFE techniques. Two microelectrodes configurations were constructed to evaluate the selectivity, LOD, reproducibility and lifetime. Overall, the zinc SC-µ-ISE exhibited good stability and durability to monitor Zn^{2+} concentrations in the vascular bundle of citrus leaves in-situ. This is the first to show Zn^{2+} transport to the citrus plants using microelectrode techniques, providing an alternative to destructive methods. The quantification of the Zn^{2+} uptake will lead to better nutritional therapy for effective HLB mitigation.

3.2 Experimental Section

3.2.1 Materials and Reagents.

Tetrabutylthiuram disulfide (Zinc Ionophore I, ZnI), potassium tetrakis [3, 5-bis-(trifluoromethyl) phenyl]borate (KTFPB) and 2-nitrophenyl octyl ether (o-NPOE), all Selectophore grade, were obtained from SigmaAldrich, USA. Potassium nitrate (KNO_3), calcium nitrate tetrahydrate ($Ca(NO_3)_2$ $4H_2O$), nitric acid (HNO_3), sodium hydroxide (NaOH), copper (II)

nitrate, ACS reagent, 99.0%, poly-(3-octylthiophene-2,5-diyl) (POT), high molecular weight polyvinyl chloride (PVC), tetrahydrofuran (THF) and N-N dimethyltrimethyl-silyamine (TMSDMA) were all obtained from Sigma-Aldrich, USA. Methylene chloride (CH_2Cl_2), chloroform ($CHCl_3$), acetone ($(CH_3)_2CO$), sulfuric acid (H_2SO_4), zinc nitrate hexahydrate 99% (metal basis), 0.2 mm dia. gold wire 99.9% (metal basis), micropipette tips (0504357) were all obtained from Fisher Scientific, USA. All solutions were prepared using deionized water purified by a Millipore Milli-Q (Billerica, MA).

3.2.2. Zinc Ion-Selective Membrane Cocktail

The Zn^{2+} cocktail was prepared by following a previously investigated composition with some modifications [13]. Zinc cocktail was prepared on a 100 mg scale that consists of 80 mmol/kg of Zn (I), 10 mmol/kg of KTFPB, (66.6 w%) o-NPOE and (33.3 w%) PVC, was dissolved in 1 mL of THF and vortexed for 1 h.

3.2.3 Preparation of Zn^{2+} SC-µ-ISEs

Two configurations of zinc SC-m-ISE were prepared using the zinc ion selective membrane cocktail described above. The configurations of the Zn^{2+} SC-µ-ISE are shown in Scheme 1. The first configuration will be denoted as SC-µ-ISE **1** and the second configuration will be denoted as SC-µ-ISE **2**. The SC-µ-ISE **1** was prepared by employing a commercially available micropipette tip (0.540 mm diameter), where a gold wire (0.20 mm diameter) coated with POT was introduced and sealed from the top with a hot melt adhesive. The zinc cocktail was inserted through capillary action and a round-like membrane formed at the end of the tip. SC-µ-ISE **2** was prepared using borosilicate glass micropipettes (Sutter Instrument Company, BF120-69-15) (ID:

0.69 mm, OD: 1.2 mm, length: 15 cm), which were pulled horizontally using a Flame/Brown type micropipette puller (Sutter Instrument Company, Model P-100).

The tip of the glass micropipette was broken with a fine tweezer to create a tip diameter between 30–100 µm and bevelled at a 45º angle using a beveller (BV-10, Sutter Instruments). The hydrophobic ion exchange membrane must adhere to the glass of the electrode to prevent the aqueous electrolyte solution from finding a pathway along the glass and short-circuiting the sensor [14]. Therefore, the glass inner surface was silanized to promote good adhesion with the hydrophobic membrane. Thus, the glass tip was dipped into TMSDMA for 15–30 sec. The micropipettes were then placed in a stainless steel mini-rack which was tightly closed by a glass container and placed in an oven at 180ºC for at least 24 hours. Then, the custom designed holder with the micropipette tips facing up was removed from the oven and a small amount (0.25 ml) of dry TMSDMA was injected quickly into the small container using a syringe. The silanization reagent evaporated immediately and the vapor reached the inner surface of the micropipette tips. The glass container was then kept in the dark in a desiccator for 1.5–2 hours before applying the ion exchange membrane. The microelectrode tip was then dipped in the Zn^{2+} ion selective membrane cocktail for 10 sec and a 100 µm POT coated gold microelectrode was position within the membrane and held in place using hot melt adhesive before the membrane was allowed to dry. The POT coated gold microelectrode was prepared ahead of time by attaching a 100 µm gold wire to a copper wire using silver paste and encasing the gold wire in borosilicate glass using the micropipette puller.

The tip of the glass was broken to expose approx. 500 µm-length of gold wire which was coated with POT solution and allowed to dry for 2 hours. After the SC-µ-ISE **2** was assembled and

allowed to dry, the tip was observed under a microscope to insure the membrane had good contact with the POT coated gold electrode.

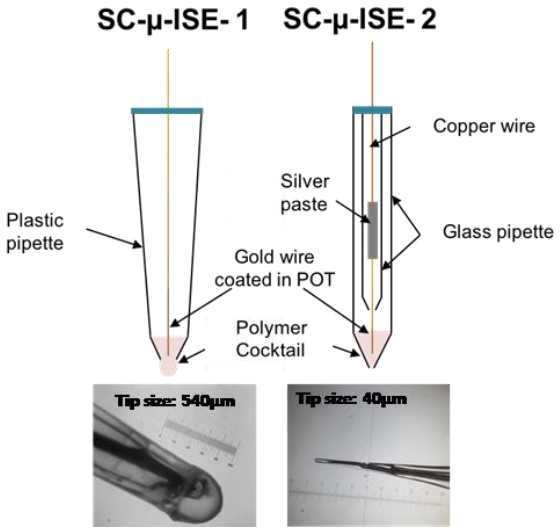

Scheme 1. Diagram and photograph of SC-µ-ISE **1** (left) and SC-µ-ISE **2** (right)

3.2.4 Characterization of Zn^{2+} SC-µ-ISE

SC-µ-ISE **1** were conditioned in a $1x10^{-3}$ M $Zn(NO_3)_2$ solution for 5 h. During measurement, the microelectrodes required a 20 min hydration time in DI water, followed by 8 min equilibration time upon analyte spiking. SC-µ-ISE **2** was conditioned in a more concentrated solution of 0.1 M $Zn(NO_3)_2$ solution for 30 min to accelerate the condition time. SC-µ-ISE **2** was allowed to hydrate in DI water for 5 minutes, followed by 2 min equilibration time between analyte spiking. Potentials for SC-µ-ISE **1** were monitored with a high input impedance (1015 Ω) EMF-16 multichannel data acquisition system (Precision Electrochemistry EMF Interface, Lawson Laboratories, Malvern, PA) at room temperature (22ºC), while stirring the solution. All measurements were conducted in a Faraday cage to minimize electrical interference and measured against a double junction Ag/AgCl/3 M KCl/1MLiOAc reference electrode (Metrohm AG). The SC-µ-ISE **1** was employed to determine pH stability and selectivity studies. Limit of

Detection (LOD) was determined experimentally using a protocol highlighted in works by Bulhman [15] and Bakker [16].

3.2.5. Determination of Ion Fluxes

Potentials for SC-µ -ISE **2** were monitored using a microsensor multimeter (Unisense A/S, Denmark) at room temperature under constant stirring. A Ag/AgCl reference electrode was used for all foliar uptake measurements. Net ion flux experiments were done after the leave/root had been exposed to Zn^{2+} solutions for 30 minutes. A custom flow cell (5 mL) was attached to the leaves of sour orange seedlings (Approx. 100 cm tall) as demonstrated in Scheme 2. A 0.5 ml/min flow of Zn^{2+} solutions ranging from 0 to 15.3 mM was used to keep the system at equilibrium. The developed Zn^{2+} SC-µ-ISE **2** was positioned using a three- dimensional micromanipulator (UNISENSE A/S, Denmark) and observed using a stereomicroscope with a CCD camera (World Precision Instruments, Sarasota, FL). The Ag/AgCl reference electrode was fixed in the flow cell using a helping hand. Data acquisition software was used to control and record the microprofiles (Sensor Trace Pro, Unisense A/S, Denmark). The experiment took place in a Faraday cage to minimize electrical interference. The microelectrode tip was moved in a direction perpendicular to the leaf surface and microprofile measurements were taken at 50 µm intervals from 1,000 to 50 µm above the surface (to avoid breaking the sensor tip). A single profile was completed in 3 minutes (<10 s response time).

When ions are taken up by living cells, the concentration in the proximity of the cell's surface will be lower than that further away [10a]. The conversion of concentration gradient data into flux estimate requires assumptions about the mechanisms of ion transport to the plant surface and the nature of the diffusion boundary layer (DBL) [10a]. However, several studies have shown planar

diffusion is mostly responsible for EMF gradients as a microelectrode approaches the surface of plant tissues [11c,17]. Therefore, only planar diffusion will be considered in this study. If ordinary diffusion is the only driving force for ion movement toward a plant surface; Fick's First Law can be used to express the proportionality between flux and concentration gradient as shown in equation 1:

$$J_{Zn^{2+}}=\frac{D(C_1-C_2)}{(X_1-X_2)} \quad (3 - 1)$$

Where, J is the net Zn^{2+} flux (in nanomoles per square centimeter per second), D is the diffusion constant for Zn^{2+} ($7.05x10^{-6}$ $cm^{-2}s^{-1}$) [18], C_1 and C_2 are the measured Zn^{2+} concentrations at X_1 and X_2, and X is the distance from the surface of the plant tissue. The minus sign is normally omitted for uptake measurements so that influx is defined as positive.

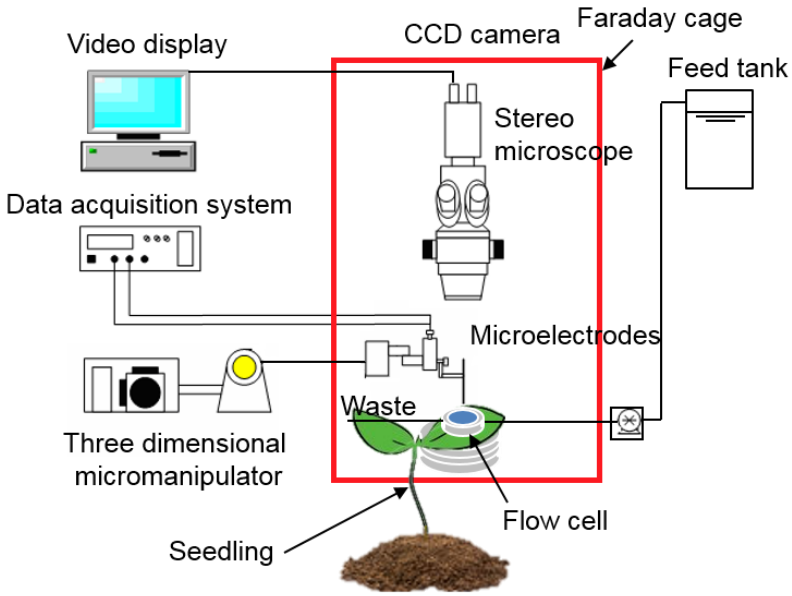

Scheme 2. Schematic diagram of micro profiling set-up for flux determination of zinc foliar/root uptake

3.3 Results and Discussion

3.3.1 Sensor Characterization

3.3.1.1 Electrode Response Towards Zn^{2+} Between SC-µ-ISE 1 and SC-µ-ISE 2

The SC-µ-ISE 1 conditioning protocol was optimized to a minimum conditioning time of 5 hour in $1x10^{-3}$ M $Zn(NO_3)_2$ yielding a Nernstian slope of 32.28 ±1.29 mVdecade^{-1} with a (2.83±0.47) $x10^{-7}$ M LOD (Figure 13A), which resembles that of the macro-ion selective electrode platform previously investigated [13]. Thus, size reduction did not hinder the electrodes ideal response. In a similar fashion, SC-µ-ISE **2** yielded a Nernstian response of 26.05±0.13 mV decade^{-1} with an LOD of (3.96±2.09) $x10^{-7}$ M (Figure 13B). For in situ determination of foliar uptake of Zn^{2+} in citrus plants, the SC-µ-ISE **2** was chosen due to its micro-sized dimensions (tip diameter 30–100 µm), allowing to maneuver various distances for flux analysis at micro-scale.

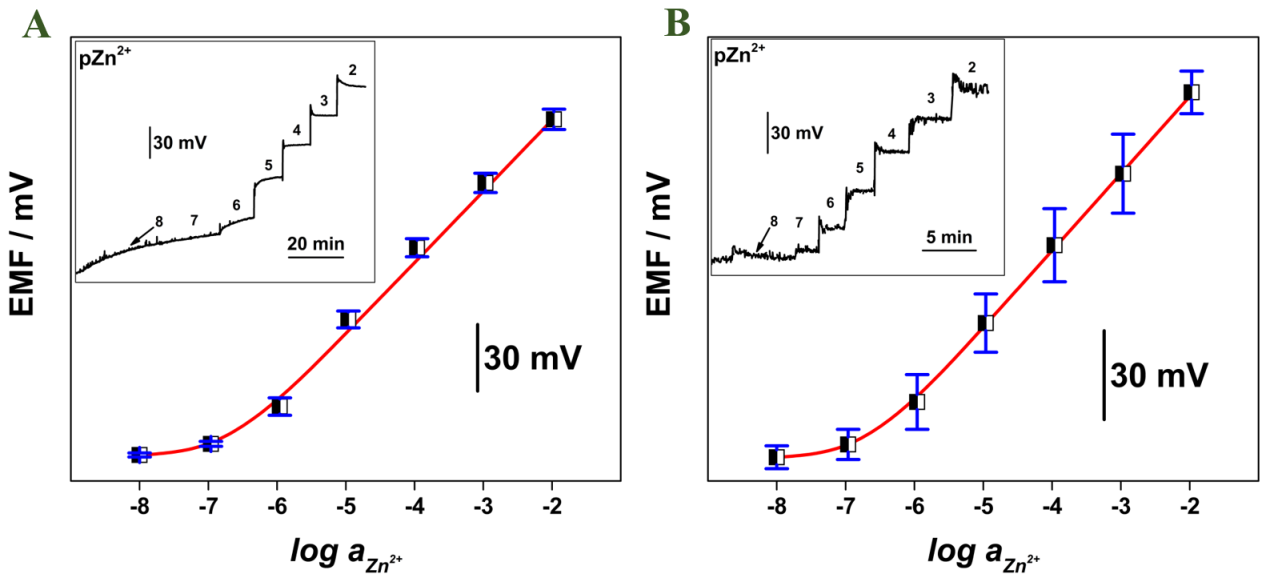

Figure 13. Zn^{2+} calibration curves with (A) SC-µ-ISE and (B) SC-µ-ISE 2. (Inset: recorded potential time traces of respective SC-u-ISEs). All measurements were done in triplicates.

3.3.1.2 pH Measurements

Given that the pH in phloem bundles in citrus plants is around 6.0 [19], the response of the sensor with fixed concentration of $Zn(NO_3)_2$ ($1x10^{-3}$ M) at varied pH was investigated. The desired pH was achieved by adjusting with either HNO_3 or NaOH (pH ranged from 2 to 9). The electrode exhibited a stable response between pH 4.00 to 7.00 as shown in Figure 14. Therefore, the proposed sensor is able to be used for MIFE analysis.

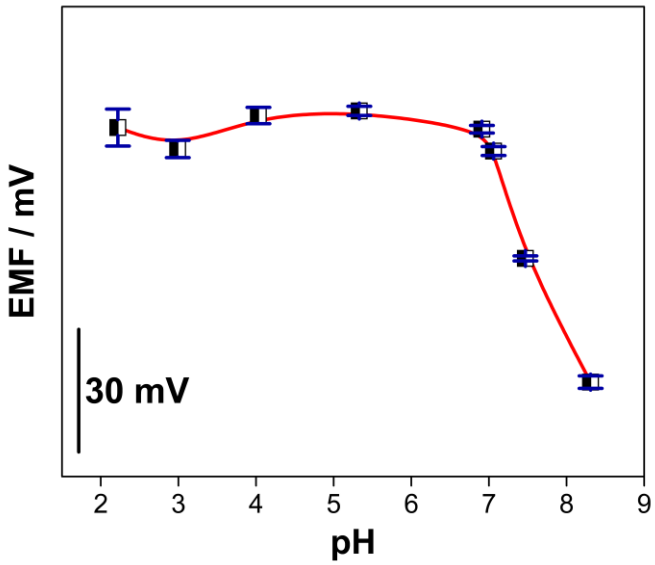

Figure 14. pH stability of Zn^{2+} SC-µ-ISE 1. Measurements were conducted in triplicates

3.3.1.3 Selectivity Coefficients

Selectivity measurements for Zn^{2+} ISEs were obtained using the unbiased separate solutions method as described by Bakker [20]. Briefly, electrodes were conditioned in the least interfering ion to obtain Nernstian response, a requirement to use Nicolskii-Eisenman equation. The slopes and selectivity coefficients are displayed in Table 2. The selectivity coefficients reported in this work varies from previously reported literature [13], since unbiased method was used.

Nonetheless, the analysis of zinc foliar uptake is conducted through a surface profile and the inference caused by copper will be highly reduced. See Table 2.

Table 2. Observed experimental selectivity coefficients

Ion $J^{(z+)}$	$K_{Zn,J}^{pot}$	**Slope (mV decade^{-1})**
Ca^{2+}	-3.15±0.07	27.10±0.53
K^{+}	2.13±0.17	52.28±2.05
H^{+}	-0.52±0.13	51.39±0.79
Cu^{2+}	10.82±0.61	38.95±5.11
Zn^{2+}	0	27.78±1.23

3.3.2 Surface Profiling

3.3.2.1 Foliar Zn^{2+} Uptake

The surface profiles of various Zn^{2+} concentrations on sour orange seedling leaves are shown in Figure 15A. There was no detectable change in concentration from the bulk solution to the leaf surface when the bulk concentration was 0, 0.2, or 1.3 mM. This likely means that the concentration gradient between the internal leaf concentration and bulk concentration was not large enough to induce Zn^{2+} flux. When the concentration of the bulk solution was 6.0 mM, there was a decrease in concentration from the bulk to the surface of the leaf by 1.6 mM. This indicates the uptake of zinc by the leaves. This trend continues with higher bulk concentrations of Zn^{2+} When the measured bulk concentration was 15.2 mM, the surface concentration was reduced to 9.1 mM.

3.3.2.2 Root Zn^{2+} Uptake

The surface profiles of Zn^{2+} uptake by the roots of a sour orange seedling are shown in Figure 15B. It is clear that there is a significant difference between Zn^{2+} uptake by roots compared to leaves. Zn^{2+} concentrations averaging 6.3 mM and 12.6 mM in the bulk were both reduced to 0.2 mM at the surface of the leaves. The DBL was also significantly different between the surface profiles of the leave and the roots. For example, with a bulk concentration of 15.2 mM, the DBL of the leaf profile was 210 µm, yet with a similar bulk concentration (12.6 mM), the DBL of the root profile was increased to 274 µm. This may be due to the geometry of the roots. Unlike the leaves, the roots are round; therefore, a slight change in profiling location can lead to large changes hydrodynamics and mass transfer.

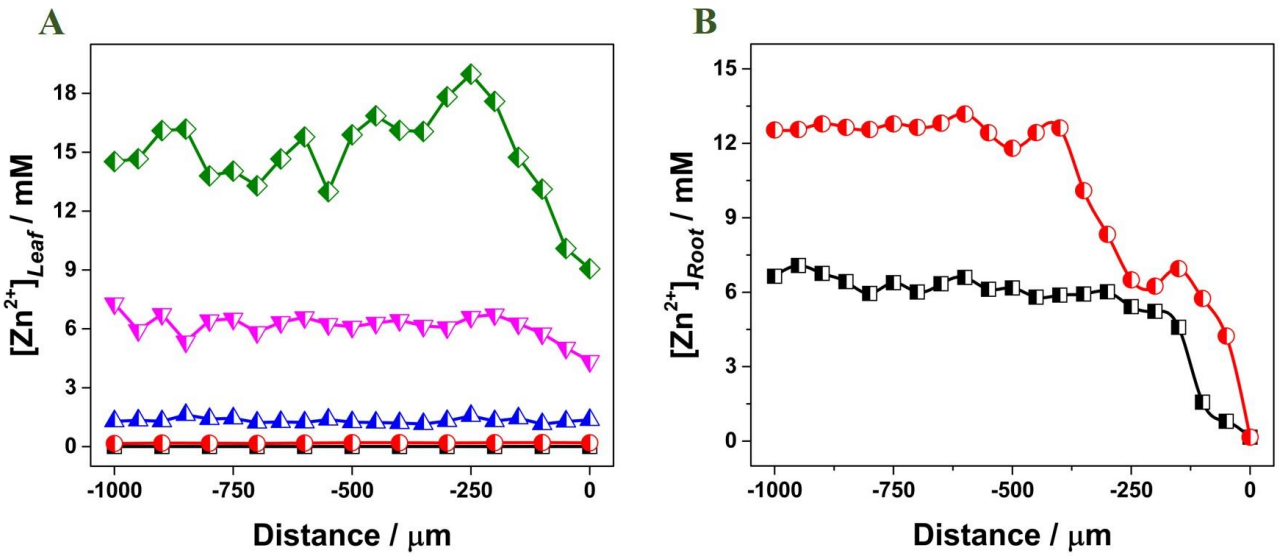

Figure 15. Microprofiles of various Zn^{2+} bulk concentration using SC-µ-ISE 2 on A) leaves and B) roots of sour orange seedlings. (On Figure 15A black squares indicate 0mM, red circles 0.20mM, blues triangles 1.3mM, pink triangles 6.0mM, and green rhombus 15.2mM Zn^{2+}. On Figure 15B black squares indicate 6.3mM and red circles 13.0mM Zn^{2+}).

3.3.1.3 Estimation of Zn^{2+} Flux via MIFE

There is contradicting research on the uptake of Zn^{2+} in the leaves of plants. Some studies show that foliar uptake is possible in wheat plants [21]; while others report foliar uptake does not occur and can leave the roots starved of Zn^{2+} if not supplied in the root environment [22]. In this study, the flux of Zn^{2+} into the leaves and roots of a sour orange seedling was calculated from the surface profiles, as shown in Figures 15 and Table 3. There was no significant flux into the leaves when bulk concentrations were 0, 0.2, or 1.3 mM. This differs from a study by Haslett et al., where the foliar uptake of zinc (as ZnO and ZnEDTA) in wheat was observed at 1 mM concentrations of zinc [16]. However, results in this study demonstrate that when bulk concentrations increased to 6.0 and 15.2 mM, Zn^{2+} transport into the leaves was observed. The Zn^{2+} flux into the leaves ranged from $5.9x10^2$ nmol $cm^{-2}s^{-1}$ to $1.73x10^3$ $nmolcm^{-2}$ for zinc concentrations of 6.0 and 15.2 mM, respectively. This shows that foliar zinc uptake is possible in sour orange leaves. Zn^{2+} flux of similar bulk concentrations was observed to be higher in the roots than compared to the leaves, indicating higher zinc uptake by the roots. The observed results were expected considering most nutrients are absorbed by the roots of plants [23]. The flux of Zn^{2+} into the leaves had a linear relationship with bulk Zn^{2+} from 1.3 mM to 15.2 mM (Figure 16), suggesting passive diffusion. However, facilitated diffusion or active transport is also likely to be involved in Zn^{2+} uptake by plants [24]. In this case, we would expect to see a saturation point where all active sites are being consumed. Research by Zhang and Brown [25] looked at foliar Zn^{2+} uptake in Pistachio and Walnut leaves and found a saturation point at >7.5 mM and 15 mM in pistachio and walnut leaves, respectively. Therefore, it is likely that there is a

saturation point in citrus plants that is higher than 15.2 mM or that the initial uptake mechanism of Zn^{2+} is passive diffusion.

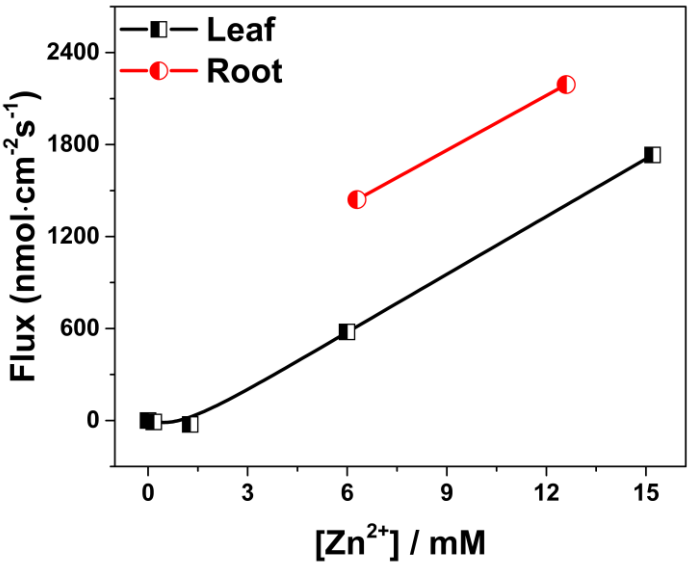

Figure 16. Zn^{2+} flux as a function of bulk concentration in leaves and roots of sour orange citrus seedlings using the developed SC-μ-ISE **2**.

Table 3. Estimated flux of Zn^{2+} into leaves and roots of sour orange seedlings using the developed SC-μ-ISE 2.

Location	**Zn^{2+}bulk concentration (mM)**	**Diffusion Boundary Layer (μm)**	**Flux**
Leaf	0	N.D.	N.D.
Leaf	0.2	N.D.	N.D.
Leaf	1.3	N.D.	N.D.
Leaf	6.0	121	$5.9x10^2$
Leaf	15.3	210	$1.7x10^3$
Root	6.3	239	$1.4x10^3$
Root	12.6	274	$2.2x10^3$

3.4 Conclusion

A Zn^{2+} SC-μ-ISE was developed and characterized for the investigation of ion-transport processes in the foliage and roots of citrus plants. The sensor displayed a 26.05±0.13 mV decade^{-1} Nernstian response and a LOD of (3.96±2.09) x10^{-7} M. Even though selectivity coefficients showed an interfering response to Cu^{2+} ($K_{Zn,J}^{pot}$=10.82±0.61); Cu^{2+} concentrations were controlled in the flux estimation experiments. Therefore, Cu^{2+} interference was considered to be reduced. It was also found that the tip size, between 40 and 540 μm did not affect the response of the sensor. Application of the developed Zn^{2+} SC-μ-ISE to the sour orange seedling revealed important information on zinc transport processes. It was found that Zn^{2+} flux is possible in citrus trees at bulk concentrations above 5.99 mM via MIFE. However, at low concentrations zero or negative flux was observed. Furthermore, the observed linear relationship between flux and bulk concentration, highlighting passive diffusion, may be a key mechanism for Zn^{2+} transport into plants. Overall, this study is the first to develop a Zn^{2+} microelectrode for the determination of ion transport processes in plants. This novel tool can be used to further knowledge on the effect of nutrient therapy on HLB infected citrus plants. Future prospects will seek to target localized detection of zinc for further information about the role of zinc as a nutritional therapy for HLB infected plants.

3.5 References

[1] a) J. M. Bove ´, J. Plant Pathol. 2006, 7–37; b) T. R. Gottwald, Annu. Rev. Phytopathol. 2010, 48, 119–139.

[2] a) E. Etxeberria, P. Gonzalez, D. Achor, G. Albrigo, Physiol. Mol. Plant Pathol. 2009, 74, 76–83; b) J.-S. Kim, U. S. Sagaram, J. K. Burns, J.-L. Li, N. Wang, Phytopathology 2009, 99, 50–57.

[3] J. d. Graca, Annu. Rev. Phytopathol. 1991, 29, 109–136.

[4] C. C. Nwugo, H. Lin, Y. Duan, E. L. Civerolo, BMC Plant Biol. 2013, 13, 59.

[5] S. Tian, L. Lu, J. M. Labavitch, S. M. Webb, X. Yang, P. H. Brown, Z. He, J. Exp. Bot. 2014, 65, 953–964.
[6] Y. Xia, G. Ouyang, R. A. Sequeira, Y. Takeuchi, I. Baez, J. Chen, Plant Health Progress 2011.
[7] T. Gottwald, J. Graham, M. Irey, T. McCollum, B. Wood, Crop Prot. 2012, 36, 73–82. [8] Handbook of Reference Methods for Plants Analysis, 4 ed., Taylor & Francis Group, Boca Raton, FL, 1998.
[9] a) A. J. Miller, S. J. Cookson, S. J. Smith, D. M. Wells, J. Exp. Bot. 2001, 52, 541–549; b) A. J. Miller, S. J. Smith, J. Exp. Bot. 1996, 47, 843–854.
[10] a) I. Newman, Plant Cell Environ. 2001, 24, 1–14; b) I. A. Newman, L. V. Kochian, M. A. Grusak, W. J. Lucas, Plant Physiol. 1987, 84, 1177–1184.
[11] a) L. V. Kochian, J. E. Shaff, W. M. Ku ¨htreiber, L. F. Jaffe, W. J. Lucas, Planta 1992, 188, 601–610; b) M. A. Pineros, J. E. Shaff, L. V. Kochian, Plant Physiol. 1998, 116, 1393–1401; c) G. H. Henriksen, D. R. Raman, L. P. Walker, R. M. Spanswick, Plant Physiol. 1992, 99, 734–747; d) S. N. Shabala, I. A. Newman, J. Morris, Plant Physiol. 1997, 113, 111–118.
[12] a) K. Y. Chumbimuni-Torres, N. Rubinova, A. Radu, L. T. Kubota, E. Bakker, Anal. Chem. 2006, 78, 1318–1322; b) U. Guth, F. Gerlach, M. Decker, W. Oelssner, W. Vonau, J. Solid State Electrochem. 2009, 13, 27–39.
[13] R. Kojima, S. Kamata, Anal. Sci. 1994, 10, 409–412.
[14] Z. L. H. Beyenal, Fundamentals of Biofilm Research, Second Edition ed., CRC Press Taylor & Francis Group, 2013.
[15] P. Bu ¨hlmann, L. D. Chen, Supramolecular Chemistry: From Molecules to Nanomaterials, John Wiley & Sons, Ltd, 2012.
[16] E. Bakker, P. Bu ¨hlmann, E. Pretsch, Chem. Rev. 1997, 97, 3083–3132.
[17] S. Shabala, O. Babourina, I. Newman, J. Exp. Bot. 2000, 51, 1243–1253.
[18] W. E. Price, L. A. Woolf, K. R. Harris, J. Phys. Chem. 1990, 94, 5109–5114.
[19] F. Hijaz, N. Killiny, PLoS One 2014, 9, 11.
[20] E. Bakker, Anal. Chem. 1997, 69, 1061–1069.
[21] B. S. Haslett, R. J. Reid, Z. Rengel, Ann Bot-London 2001, 87, 379–386.
[22] M. J. Webb, J. F. Loneragan, J. Plant Nutr. 1990, 13, 1499– 1512.
[23] N. Gupta, H. Ram, B. Kumar, Rev. Environ. Sci. Bio/ Technol. 2016, 15, 89–109.
[24] W. H. Jyung, S. H. Wittwer, M. J. Bukovac, PAm Soc Hortic Sci 1965, 86, 361.
[25] Q. L. Zhang, P. H. Brown, J. Am. Soc. Hortic. Sci. 1999, 124, 312–317.

APPENDIX A: SUPPORTING INFORMATION FOR CHAPTER THREE

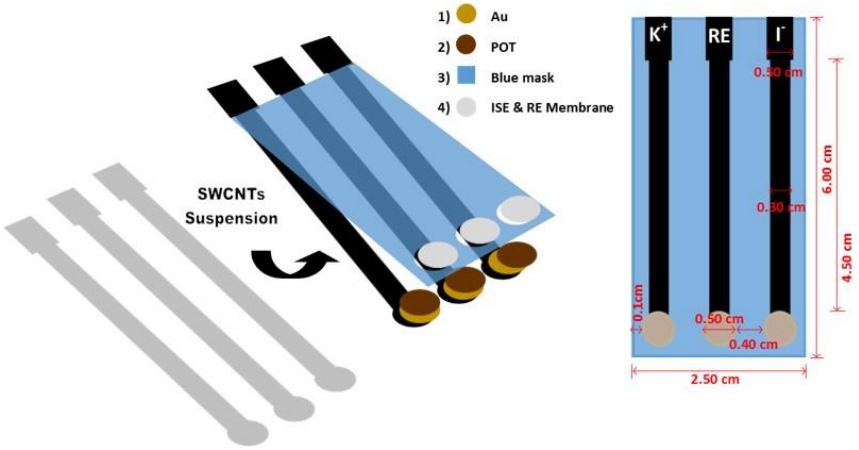

Figure 2A-1. Schematic Diagram of the preparation of the multiplex PBSC-ISE platform

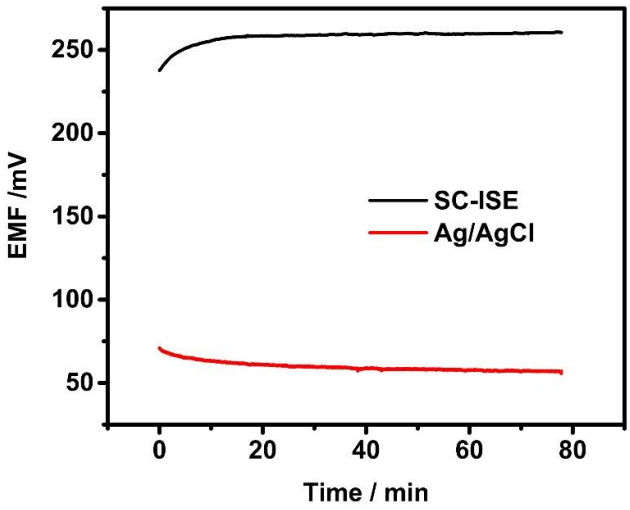

Figure 2A-2. Hydration of solid-contact reference electrode and commercial single junction Ag/AgCl reference electrode versus double junction Ag/AgCl/3MKCl/1MLiOAc in aqueous solution.

One crucial characteristic for reference electrodes lies in their potential stability over time, particularly avoiding potential drifts. Additionally, it is important for reference electrodes to achieve equilibrium with the aqueous face via high free energy of hydration for fast response and analysis. Hydration allows ions from the organic phase to equilibrate with ions of the aqueous phase, ease solvation, and reach a thermodynamic equilibrium. Here, we show the trace of potential versus time graph, where the proposed solid-contact reference electrode is compared to

a commercial single junction Ag/AgCl reference electrode. As seen, the response and stability of the solid-contact electrodes agree with that expected for a commercial reference electrode.

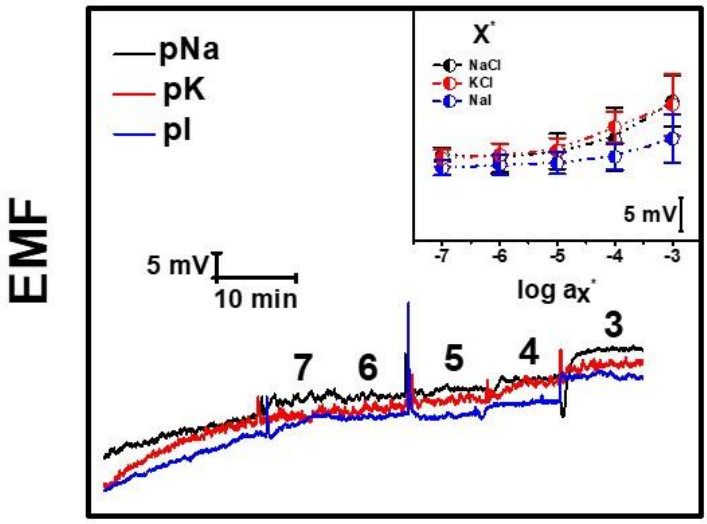

Figure 2A-3. Response of solid-contact electrode against commercial single-junction Ag/AgCl reference electrode

APPENDIX B: COPYRIGHT PERMISSION

Chapter 2 adapted with permission from:

Copyright Clearance Center RightsLink®

Home | Account Info | Help

Title: Ready-to-use single-strip paper based sensor for multiplex ion detection

Author: Stephanie M. Armas,Andrew J. Manhan,Olivia Younce,Percy Calvo-Marzal,Karin Y. Chumbimuni-Torres

Publication: Sensors and Actuators B: Chemical

Publisher: Elsevier

Date: February 2018

© 2017 Elsevier B.V. All rights reserved.

Logged in as:
Stephanie Armas
Account #:
3001232441

LOGOUT

Please note that, as the author of this Elsevier article, you retain the right to include it in a thesis or dissertation, provided it is not published commercially. Permission is not required, but please ensure that you reference the journal as the original source. For more information on this and on your other retained rights, please visit: https://www.elsevier.com/about/our-business/policies/copyright#Author-rights

BACK | CLOSE WINDOW

Copyright © 2018 Copyright Clearance Center, Inc. All Rights Reserved. Privacy statement. Terms and Conditions.
Comments? We would like to hear from you. E-mail us at customercare@copyright.com

Chapter 3 adapted with permission from: (Page 1 of 5)

JOHN WILEY AND SONS LICENSE TERMS AND CONDITIONS

May 05, 2018

This Agreement between 9822 Piney Point Circl ("You") and John Wiley and Sons ("John Wiley and Sons") consists of your license details and the terms and conditions provided by John Wiley and Sons and Copyright Clearance Center.

License Number	4257220320612
License date	Dec 27, 2017
Licensed Content Publisher	John Wiley and Sons
Licensed Content Publication	Electroanalysis
Licensed Content Title	Development and Characterization of Needle-Type Ion-Selective Microsensors for in situ Determination of Foliar Uptake of Zn2+ in Citrus Plants
Licensed Content Author	Jared Church,Stephanie M. Armas,Parth K. Patel,Karin Chumbimuni-Torres,Woo Hyoung Lee
Licensed Content Date	Dec 4, 2017
Licensed Content Pages	1
Type of use	Dissertation/Thesis
Requestor type	Author of this Wiley article
Format	Electronic
Portion	Full article
Will you be translating?	No
Title of your thesis / dissertation	Development and characterization of solid-contact paper-based and micro ion-selective electrodes for enviromental analysis
Expected completion date	Jul 2018
Expected size (number of pages)	70
Requestor Location	Stephanie M. Armas 9822 Piney Point Circle ALAFAYA, FL 32816 United States Attn: N/A
Publisher Tax ID	EU826007151
Billing Type	Invoice
Billing Address	9822 Piney Point Circl 9822 Piney Point Circle ALAFAYA, FL 32816 United States Attn: 9822 Piney Point Circl
Total	0.00 USD

Chapter 3 adapted with permission from: (Page 2 of 5)

- The Wiley Materials and all of the intellectual property rights therein shall at all times remain the exclusive property of John Wiley & Sons Inc, the Wiley Companies, or their respective licensors, and your interest therein is only that of having possession of and the right to reproduce the Wiley Materials pursuant to Section 2 herein during the continuance of this Agreement. You agree that you own no right, title or interest in or to the Wiley Materials or any of the intellectual property rights therein. You shall have no rights hereunder other than the license as provided for above in Section 2. No right, license or interest to any trademark, trade name, service mark or other branding ("Marks") of WILEY or its licensors is granted hereunder, and you agree that you shall not assert any such right, license or interest with respect thereto

- NEITHER WILEY NOR ITS LICENSORS MAKES ANY WARRANTY OR REPRESENTATION OF ANY KIND TO YOU OR ANY THIRD PARTY, EXPRESS, IMPLIED OR STATUTORY, WITH RESPECT TO THE MATERIALS OR THE ACCURACY OF ANY INFORMATION CONTAINED IN THE MATERIALS, INCLUDING, WITHOUT LIMITATION, ANY IMPLIED WARRANTY OF MERCHANTABILITY, ACCURACY, SATISFACTORY QUALITY, FITNESS FOR A PARTICULAR PURPOSE, USABILITY, INTEGRATION OR NON-INFRINGEMENT AND ALL SUCH WARRANTIES ARE HEREBY EXCLUDED BY WILEY AND ITS LICENSORS AND WAIVED BY YOU.

- WILEY shall have the right to terminate this Agreement immediately upon breach of this Agreement by you.

- You shall indemnify, defend and hold harmless WILEY, its Licensors and their respective directors, officers, agents and employees, from and against any actual or threatened claims, demands, causes of action or proceedings arising from any breach of this Agreement by you.

- IN NO EVENT SHALL WILEY OR ITS LICENSORS BE LIABLE TO YOU OR ANY OTHER PARTY OR ANY OTHER PERSON OR ENTITY FOR ANY SPECIAL, CONSEQUENTIAL, INCIDENTAL, INDIRECT, EXEMPLARY OR PUNITIVE DAMAGES, HOWEVER CAUSED, ARISING OUT OF OR IN CONNECTION WITH THE DOWNLOADING, PROVISIONING, VIEWING OR USE OF THE MATERIALS REGARDLESS OF THE FORM OF ACTION, WHETHER FOR BREACH OF CONTRACT, BREACH OF WARRANTY, TORT, NEGLIGENCE, INFRINGEMENT OR OTHERWISE (INCLUDING, WITHOUT LIMITATION, DAMAGES BASED ON LOSS OF PROFITS, DATA, FILES, USE, BUSINESS OPPORTUNITY OR CLAIMS OF THIRD PARTIES), AND WHETHER OR NOT THE PARTY HAS BEEN ADVISED OF THE POSSIBILITY OF SUCH DAMAGES. THIS LIMITATION SHALL APPLY NOTWITHSTANDING ANY FAILURE OF ESSENTIAL PURPOSE OF ANY LIMITED REMEDY PROVIDED HEREIN.

- Should any provision of this Agreement be held by a court of competent jurisdiction to be illegal, invalid, or unenforceable, that provision shall be deemed amended to achieve as nearly as possible the same economic effect as the original provision, and the legality, validity and enforceability of the remaining provisions of this Agreement

Chapter 3 adapted with permission from: (Page 3 of 5)

Chapter 3 adapted with permission from: (Page 4 of 5)

shall not be affected or impaired thereby.

- The failure of either party to enforce any term or condition of this Agreement shall not constitute a waiver of either party's right to enforce each and every term and condition of this Agreement. No breach under this agreement shall be deemed waived or excused by either party unless such waiver or consent is in writing signed by the party granting such waiver or consent. The waiver by or consent of a party to a breach of any provision of this Agreement shall not operate or be construed as a waiver of or consent to any other or subsequent breach by such other party.

- This Agreement may not be assigned (including by operation of law or otherwise) by you without WILEY's prior written consent.

- Any fee required for this permission shall be non-refundable after thirty (30) days from receipt by the CCC.

- These terms and conditions together with CCC's Billing and Payment terms and conditions (which are incorporated herein) form the entire agreement between you and WILEY concerning this licensing transaction and (in the absence of fraud) supersedes all prior agreements and representations of the parties, oral or written. This Agreement may not be amended except in writing signed by both parties. This Agreement shall be binding upon and inure to the benefit of the parties' successors, legal representatives, and authorized assigns.

- In the event of any conflict between your obligations established by these terms and conditions and those established by CCC's Billing and Payment terms and conditions, these terms and conditions shall prevail.

- WILEY expressly reserves all rights not specifically granted in the combination of (i) the license details provided by you and accepted in the course of this licensing transaction, (ii) these terms and conditions and (iii) CCC's Billing and Payment terms and conditions.

- This Agreement will be void if the Type of Use, Format, Circulation, or Requestor Type was misrepresented during the licensing process.

- This Agreement shall be governed by and construed in accordance with the laws of the State of New York, USA, without regards to such state's conflict of law rules. Any legal action, suit or proceeding arising out of or relating to these Terms and Conditions or the breach thereof shall be instituted in a court of competent jurisdiction in New York County in the State of New York in the United States of America and each party hereby consents and submits to the personal jurisdiction of such court, waives any objection to venue in such court and consents to service of process by registered or certified mail, return receipt requested, at the last known address of such party.

WILEY OPEN ACCESS TERMS AND CONDITIONS

Chapter 3 adapted with permission from: (Page 5 of 5)

Wiley Publishes Open Access Articles in fully Open Access Journals and in Subscription journals offering Online Open. Although most of the fully Open Access journals publish open access articles under the terms of the Creative Commons Attribution (CC BY) License only, the subscription journals and a few of the Open Access Journals offer a choice of Creative Commons Licenses. The license type is clearly identified on the article.

The Creative Commons Attribution License

The Creative Commons Attribution License (CC-BY) allows users to copy, distribute and transmit an article, adapt the article and make commercial use of the article. The CC-BY license permits commercial and non-

Creative Commons Attribution Non-Commercial License

The Creative Commons Attribution Non-Commercial (CC-BY-NC)License permits use, distribution and reproduction in any medium, provided the original work is properly cited and is not used for commercial purposes.(see below)

Creative Commons Attribution-Non-Commercial-NoDerivs License

The Creative Commons Attribution Non-Commercial-NoDerivs License (CC-BY-NC-ND) permits use, distribution and reproduction in any medium, provided the original work is properly cited, is not used for commercial purposes and no modifications or adaptations are made. (see below)

Use by commercial "for-profit" organizations

Use of Wiley Open Access articles for commercial, promotional, or marketing purposes requires further explicit permission from Wiley and will be subject to a fee.

Further details can be found on Wiley Online Library

http://olabout.wiley.com/WileyCDA/Section/id-410895.html

Other Terms and Conditions:

v1.10 Last updated September 2015

Questions? customercare@copyright.com or +1-855-239-3415 (toll free in the US) or +1-978-646-2777.